REPORT DOCUMENTATION PAGE

AFRL-SR-AR-TR-03-

0292

1. AGENCY USE ONLY *(Leave blank)*	2. REPORT DATE	3. RE
		01 Apr 1999 - 30 Sep 2002 Final Report

4. TITLE AND SUBTITLE
(DEPSCOR 99) Experimetnal Investigation of Superconducting Quantum Interference Devices as Solid State Qubits for Quantum Computing

5. FUNDING NUMBERS
61103D
3484/BS

6. AUTHOR(S)
PROFESSOR HAN

7. PERFORMING ORGANIZATION NAME(S) AND ADDRESS(ES)
UNIVERSITY OF KANSAS
CENTER FOR RESEARCH
2385 IRVING HILL ROAD
LAWRENCE KS 66044-7552

8. PERFORMING ORGANIZATION REPORT NUMBER

9. SPONSORING/MONITORING AGENCY NAME(S) AND ADDRESS(ES)
AFOSR/NE
4015 WILSON BLVD
SUITE 713
ARLINGTON VA 22203

10. SPONSORING/MONITORING AGENCY REPORT NUMBER
F49620-99-1-0205

11. SUPPLEMENTARY NOTES

12a. DISTRIBUTION AVAILABILITY STATEMENT
APPROVED FOR PUBLIC RELEASE, DISTRIBUTION UNLIMITED

12b. DISTRIBUTION CODE

13. ABSTRACT *(Maximum 200 words)*
During the past 42 months (4/1/1999 - 9/30/2002 with a 6-month no-cost extension period started from 4/1/2002) we have mostly achieved the technical goals of the project. More importantly, in addition to the scientific and technical achievements presented below, this DEPSCoR project has laid down a solid foundation for the establishment of a very competitive and successful superconducting quantum computing program at the University of Kansas.

14. SUBJECT TERMS			15. NUMBER OF PAGES
			16. PRICE CODE
17. SECURITY CLASSIFICATION OF REPORT	18. SECURITY CLASSIFICATION OF THIS PAGE	19. SECURITY CLASSIFICATION OF ABSTRACT	20. LIMITATION OF ABSTRACT
UNCLASSIFIED	UNCLASSIFIED	UNCLASSIFIED	UL

NE

Final Technical Report

Grant #F49620-99-1-0205

Submitted to AFOSR

Siyuan Han

Physics + Astronomy Department, University of Kansas

1251 Wescoe Hall Dr, Room 1082, Lawrence, KS 66045

Phone: 785-864-5831, fax: 785-864-5262, email: han@ku.edu

(Submitted on October 11th, 2002)

Objective

The objective of the proposed research is to explore the possibility of using superconducting devices based on Josephson effect, such as Josephson junctions and SQUIDs, as basic building blocks for quantum computing by investigating problems fundamental to the issue:

1. Development of time-domain measurement techniques that can be used to monitor time evolution of superconducting qubits with nanoseconds resolution.
2. Measurement of energy relaxation time (T_1) in superconducting devices. For superconducting qubits T_1 is finite because of coupling to environments. T_1 is one of the most important parameters (the other is the phase relaxation time T_2) that limit the coherence time of superconducting qubits.
3. Development of single-shot readout schemes that minimize dissipation and backaction to SQUID qubits.
4. Demonstration of coherent dynamics of superconducting qubits with the use of pulsed microwave excitation technique.

Accomplishments/New Findings

During the past 42 months (4/1/1999 – 9/30/2002 with a 6-month no-cost extension period started from 4/1/2002) we have mostly achieved the technical goals of the project.

More importantly, in addition to the scientific and technical achievements presented below, this DEPSCoR project has laid down a solid foundation for the establishment of a very competitive and successful superconducting quantum computing program at the University of Kansas. Building upon the research results obtained with the DEPSCoR support the Quantum Devices and Circuits Laboratory, led by the PI, at the Department of Physics and Astronomy has gained substantial federal research grants (~$900k) since 2000 from DoD and NSF.

Following is a list of the major results obtained with support (or partial support) from this project:

1. Investigated the microwave-SQUID interaction in strong-field regime when two-photon process has to be taken into account. This work is in collaboration with R. Rouse of Sun Microsystems and Jim Lukens of Stony Brook. The detail of this work is reported in Appendix A.
2. Developed a time-domain nanoseconds measurement technique tailored for investigating time-dependent phenomena in superconducting qubits. Detail of this work is described in Appendix B.
3. Applying this time-domain method we successfully measured the energy relaxation time, which is greater than 10 μs, in a Josephson junction qubit. This work is reported in Appendix C.
4. Investigated macroscopic quantum tunneling in dc SQUID which sets the limit on using dc SQUID as the readout device for single-shot measurement of SQUID qubit states (Appendix D). Characterized single-shot measurement of SQUID qubits with unshunted dc SQUID detectors (Appendix E).
5. Demonstrated Rabi oscillations, which is one of the key approaches of realizing quantum gates, in a NbN/Al/NbN Josephson tunnel junction with long coherence time approaching 5 μs (Appendix F). Being able to generate Rabi oscillations is a critically important step in realizing 1-bit and 2-bit quantum gates. Our result shows that not only quantum gates based on pulsed microwave induced Rabi oscillations can be used to control and manipulate superconducting solid state qubits but also that long coherence time suitable for error tolerant quantum computing can be achieved in superconducting qubits.

Prof. Shih-I Chu's group collaborated with us, through an NSF grant, in the theoretical aspect of some of the above works. The samples are provided by Dr. Zhen Wang of Communication Research Lab (Japan) through the same NSF collaboration.

Personnel Supported

- Siyuan Han (PI).
- Shao-Xiong Li (postdoc).

- Yang Yu (Ph.D. Fall 2002).
- Wei Qiu (grad. Student).
- Yu Zhang (M.S. Summer 2002).
- Zhengyu Pan (grad. student).

Peer-Reviewed Publications

1. Shao-Xiong Li, Yang Yu, Yu Zhang, Wei Qiu, Siyuan Han, and Zhen Wang, "Quantitative Study of Macroscopic Quantum Tunneling in a dc SQUID: A System with Two Degrees of Freedom", *Phys. Rev. Lett.* **89**, 098301 (2002).
2. Yang Yu, Siyuan Han, Xi Chu, Shih-I Chu, and Zhen Wang, "Coherent Temporal Oscillations of Macroscopic Quantum States in a Josephson Junction", *Science* **296**, 889 (2002).
3. Yang Yu, Yu Zhang, Wei Qiu, Shao-Xiong Li, Siyuan Han, and Zhen Wang, "Observation of the temporal evolution of an unstable macroscopic quantum system with a nanoseconds resolution", *Supercon. Sci. & Tech.* **15**, 555 (2002).
4. Siyuan Han, Yang Yu, Xi Chu, Shih-I Chu, and Zhen Wang, "Time-Resolved Measurement of Dissipation-Induced Decoherence in a Josephson Junction", *Science* **293**, 1457 (2001).
5. Siyuan Han and R. Rouse, Comment on "Measurement of the Intrinsic Dissipation of a Macroscopic System in the Quantum Regime", *Phys. Rev. Lett.* **86**, 4191 (2001).
6. Siyuan Han, R. Rouse, and J. E. Lukens, "Observation of Cascaded Two-Photon-Induced Transitions between Fluxoid States of a SQUID", *Phys. Rev. Lett.* **84**, 1300 (2000).
7. Roberto S. Aga, Yi-Yuan Xie, Shao-Lin Yan, Judy Wu, and Siyuan Han, "Microwave-power handling capability of $HgBa_2CaCu_2O_{6+\delta}$ Superconducting Microstrip Lines", *Appl. Phys. Lett.* **79**, 2417 (2002).
8. Shao-Xiong Li, Yang Yu, Wei Qiu, Siyuan Han, and Zhen Wang, "Efficiency of Unshunted dc SQUID as Readout Devices for Flux Based Qubits", submitted to *Proceedings of Applied Superconductivity Conference, IEEE Trans. Appl. Supercon.* (2002)

Interactions/Transitions

1. *Oral presentations*

- Siyuan Han, "Superconducting Phase and Flux Qubits", ARO QCPR, Nashville, TN, August 2002.
- Yang Yu, "Coherent Control of Macroscopic Quantum States in a Josephson Junction", Applied Superconductivity Conference, Houston, TX, August 2002.
- Siyuan Han, "Development of Quantum Computing using Josephson Effect Qubits", AFOSR-DURINT-QC Program Review, MIT, Boston, MA, July 2002.
- Siyuan Han, "Rabi Oscillations in a Josephson Phase Qubit", International Workshop on Macroscopic Quantum Coherence and Computing, Naples, Italy, June 2002.
- Siyuan Han, "Current Status and Future Perspective of Superconducting Quantum Computing", Kansas Center for Advanced Scientific Computing Seminar at Univ. of Kansas, April 2002.
- Siyuan Han, "Rabi Oscillations in Josephson Tunnel Junctions", AFOSR50 Superconducting Quantum Computing Workshop, Virginia Beach, VA, March 2002.
- Siyuan Han, "Qubit State Preparation and Manipulation", AFOSR-DURINT-QC kick-off meeting, Stanford University, CA, Oct. 2001.
- Siyuan Han, "Prospects of Solid State Quantum Computing", Condensed Matter Physics Seminar at Kansas State University, Sept. 2001.
- Siyuan Han, "Schrodinger's Cat, Josephson SQUID, and Quantum Computing", CMP seminar, KU, Sept. 2001.
- Siyuan Han, "Time-domain measurement of decoherence time in a Josephson tunnel junction", SUNY at Stony Brook, July 30, 2001.
- Yang Yu, Yu Zhang, Wei Qiu, Shaoxiong Li, and Siyuan Han, "Characterization of Josephson Devices using nanosecond Time Domain Measurement Technique", APS March Meeting, Seattle, WA, March 2001.

- Yang Yu, Wei Qiu, and Siyuan Han, "Measurement of Dissipation Barrier of Josephson Tunnel Junctions", APS March Meeting, Minneapolis, MN, March 2000.
- Siyuan Han, "SQUID Millimeterwave Detectors with Super Quantum Limit Performance", APS March Meeting, Minneapolis, MN, March 2000.

2. Poster presentations

- Shaoxiong Li, Yang Yu, Wei Qiu, Siyuan Han, and Zhen Wang, "Efficiency of Underdamped dc SQUIDs as Single-Shot Readout Devices for Flux Qubits", Applied Superconductivity Conference, Houston, TX, August 2002.
- Yang Yu, Shaoxiong Li, Siyuan Han, and Zhen Wang, "Low-Frequency noise in NbN Tunnel Junctions", Applied Superconductivity Conference, Houston, TX, August 2002.
- Yang Yu, Yu Zhang, Wei Qiu, Shaoxiong Li, Siyuan Han, and Zhen Wang, "Measurement of Decoherence Time of NbN Josephson Junctions", The 8th International Superconductive Conference, Osaka, Japan, June 2001.

Equipment and Infrastructure

Funds from this project also allowed us to purchase a Janis He-3 fridge with a base temperature 0.26 K, which significantly reduces the time and liquid helium required for testing and characterizing the junctions and SQUIDs at T>0.3 K.

Appendix A

Observation of Cascaded Two-Photon-Induced Transitions between Fluxoid States of a SQUID

Siyuan Han
Department of Physics and Astronomy, University of Kansas, Lawrence, Kansas 66045

R. Rouse
Sun Microsystems, Sunnyvale, California 94086

J. E. Lukens
Department of Physics and Astronomy, University at Stony Brook, Stony Brook, New York 11794-3800
(Received 21 September 1999)

We present evidence for transitions between fluxoid wells of a SQUID due to cascaded, two-photon processes. Such transitions are evidenced by an anomalous dependence on the transition rate from the one-photon resonant level within the initial well, which cannot be explained by previously observed macroscopic resonant tunneling. These two-photon processes may be a significant source of decoherence in SQUID qubits subject to microwave radiation.

PACS numbers: 74.50.+r, 03.65.−w, 85.25.Dq

The degree to which macroscopic degrees of freedom (MDFs) obey quantum mechanics is a perennial source of paradoxes and debates [1–4]. Examples of these MDFs include the center of mass of a baseball, the magnetization vector of a solid, and (the focus here) the phase difference φ of the superconducting wave function across a Josephson junction or (equivalently) the magnetic flux Φ enclosed by a SQUID. φ and Φ typically represent the collective motion of a large number ($\sim 10^{10}$) of Cooper pairs, putting them well into the "macroscopic" regime. In recent years, it has been predicted theoretically and verified experimentally that under appropriate conditions, such as low temperature and weak damping, at least some aspects of the behavior of MDFs must be described quantum mechanically [5–19]. However, the existence of a coherent superposition of states of MDFs remains largely untested. Some of the most remarkable macroscopic quantum effects, such as energy level quantization, resonant tunneling, and resonant photon assisted tunneling between macroscopically distinct levels, have been observed in Josephson junctions and SQUIDs [16,20–22]. Results from SQUID experiments have shown that SQUIDs can, in many respects, be custom designed quantum elements, which are promising for applications in fundamental scientific research (e.g., tests of macroscopic quantum coherence and macrorealism) as well as potential technological applications (e.g., qubits for quantum computing). The interaction between SQUIDs and microwave fields in the quantum regime plays an important role in many of these potential applications [23] but has only just begun to be tested. In this Letter, we report the first observation of the effect of two-photon processes on the transitions of a SQUID between its macroscopically distinct fluxoid states.

The details of the SQUID system have been reported elsewhere [24]. We summarize its key features here. Figure 1 shows the schematic and equivalent potential of a SQUID biased with an applied flux (in units of the flux quantum Φ_0) of $\phi_x \approx \frac{1}{2}$. The two wells of the potential represent the $f = 0$ and 1 fluxoid state of the SQUID, which for the parameters of our experiment, have counter circulating currents with magnitudes greater than 2 μA. The energy levels are calculated, neglecting damping, by numerical solution of Schrödinger's equation. The effect of damping on the energy of a level is of second order [25,26] and should be negligible in the low damping limit appropriate here. For $\phi_x = \frac{1}{2}$, the potential is symmetric with an energy barrier ΔU_0. As ϕ_x is varied about $\frac{1}{2}$, there is an offset ε in the energy minima of the wells, which is nearly linear in ϕ_x. This, in turn, permits a controlled shift of the relative energy of the levels in different wells. These levels (indexed by $[f, i]$) with energies $E_{f,i}$ well below the barrier are localized in either the $f = 0$ or $f = 1$ fluxoid state while levels with energy close to and above the top of the barrier are delocalized [27]. All energies are measured with respect to $E_{0,0}$—the energy

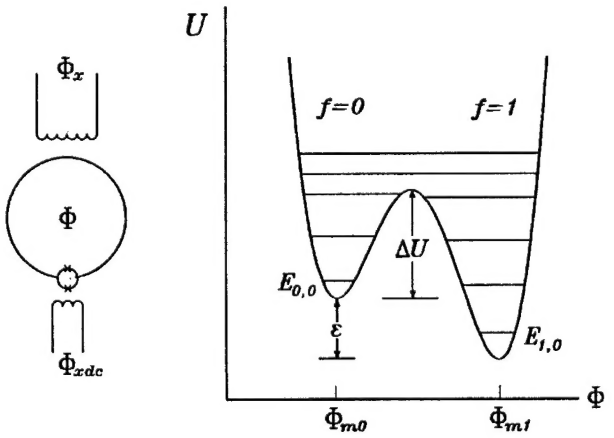

FIG. 1. Circuit schematic (left) and equivalent potential (right) describing the variable β_L SQUID.

 0031-9007/00/84(6)/1300(4)$15.00

of the lowest eigenstate of the $f = 0$ well, $[0,0]$—which we always take to be the initial state of the system. We also take ϕ_x such that $E_{0,0} \geq E_{1,0}$. The small, double-junction loop seen in Fig. 1 acts, to a good approximation, as a single junction whose critical current I_c can be modulated by changing the flux ϕ_{xdc} through the loop. We express I_c in dimensionless units using the parameter $\beta_L = 2\pi L I_c/\Phi_0$. $\beta_L(\phi_{xdc}) \simeq \beta_{L0}|\cos(\pi\phi_{xdc})|$, where β_{L0} is just the maximum value of β_L, obtained for $\phi_{xdc} = 0$. Thus the energy level spectrum $\{E_{f,i}\}$ of the SQUID can be varied by adjusting, *in situ*, ε and/or β_L.

Measurements of the transition rate Γ vs ε of the system from the upper ($f = 0$) to lower ($f = 1$) well in the presence of a small microwave magnetic field ($\nu \approx 100$ GHz) exhibit a series of resonances whose positions in ε and β_L agree very well with those obtained from the calculated energy levels only using four adjustable parameters ($L = 231 \pm 4$ pH, $C = 77 \pm 3$ fF, $\beta_{L0} = 2.01 \pm 0.005$, and $\nu = 100.8 \pm 0.5$ GHz) to describe the more than 500 peaks observed. These fitting parameters, including the SQUID inductance L and the junctions' capacitance C, are all in agreement with independently determined values.

We have previously identified two dominant transition processes for this system. One, which we call photon induced tunneling, occurs when the energy difference between a level in the $f = 1$ well and the initial state $[0,0]$ equals the photon energy of the microwave field, i.e., $E_{1,j} - E_{0,0} = h\nu$. The rates for this process can be obtained from Fermi's golden rule:

$$W^p_{i\to j} = \frac{2\pi}{\hbar}|\hat{V}_{ij}|^2\rho(E_i - E_j \pm \hbar\omega), \qquad (1)$$

where $\hat{V} = (\Phi_0^2/2L)\phi_{xrf}\hat{\phi}$, $\hat{\phi} = \hat{\Phi}/\Phi_0$, and $\phi_{xrf} = \Phi_{xrf}/\Phi_0$. Here and below, we use i to indicate levels in the $f = 0$ well and j for levels in the $f = 1$ well or above the barrier. This equation also describes pumping to excited levels within the initial well (replacing j by i'). The second process involves tunneling, at constant energy, between the wells at a rate given by

$$W^t_{i\to j} = \frac{|T_{ij}|^2}{2\hbar}\,\frac{\gamma_{ij}/2}{\Delta E_{ij}^2 + (\gamma_{ij}/2)^2}, \qquad (2)$$

where, T_{ij} is the tunneling matrix element between $|i\rangle$ and $|j\rangle$, $\gamma_{ij} = \gamma_i + \gamma_j$ is the combined linewidth of the levels involved, and ΔE_{ij} is the energy difference between the levels. The total tunneling rate from a level is just

$$\Gamma^t_i = \sum_j W^t_{i\to j} n_i, \qquad (3)$$

where n_i is the occupation of the initial state. This process has two resonances: One, which we call macroscopic resonant tunneling, occurs when $\Delta E_{ij} = 0$ for some j, though, in practice, only the final state with the minimum ΔE_{ij} contributes significantly to this process. The second, which is called resonantly activated tunneling (RAT), occurs when a level in the initial well (for our system [0,3]) is in resonance so that $n_{0,3}$ is a maximum, i.e., for $\varepsilon(\beta_L)$ such that $E_{0,3} - E_{0,0} = h\nu$. One expects the amplitude of this RAT resonance to vary periodically with β_L, having a series of local maxima for values of β_L such that the resonant tunneling condition is simultaneously satisfied.

The dissipation in the system, which we model as a resistive shunt R across the junction, enters these rates through the linewidths γ or the related density of states

$$\rho(\Delta E) = \frac{\gamma}{2\pi}\,\frac{1}{\Delta E^2 + \gamma^2/4}. \qquad (4)$$

γ is determined for all active levels (except [0,0]) by spontaneous decay to the next lower level in the same well at a rate given by

$$W^s_{i\to i'} = \frac{2\pi\Delta E_{ii'}}{\hbar}\,\frac{R_Q}{R}|\phi_{ii'}|^2\left[1 + \coth\left(\frac{\Delta E_{ii'}}{2k_BT}\right)\right], \qquad (5)$$

where, $\Delta E_{ii'} = E_i - E_{i'}$, $R_Q = h/4e^2$, and $\phi_{ii'} = \langle i|\hat{\phi}|i'\rangle$. Since the intrawell level spacing of about 1.5 K is much greater than the temperature ($T \approx 30$ K), the inverse process is negligible.

In general, it is necessary to solve the master equation to obtain the occupations n_i. In fact, for most of the parameter space studied, only two initial levels are important for interwell transitions. Since the microwave perturbation is weak and the tunneling rate small, $n_{0,0} \approx 1$. The system then undergoes photoexcitation from this level to a level near resonance in either of the wells (Γ^p). The excitation within the same well (to [0,3]) and subsequent sequential decay ($i \to i - 1$) back to [0,0] results in roughly equal populations for levels [0,3] through [0,1], ranging from about 10^{-6} to 10^{-3} for the data depending on how close to RAT resonance (as a function of ε and β_L) the system is. While we generally use a rather large set of states for the solution of the master equation, a very good estimate of n_i in the system can be obtained from the reduced master equation $W^p_{0,0\to 0,3} = n_{0,3}W^s_{0,3\to 0,2}$ together with arguments above. All other decay channels for the [0,3] levels, including stimulated emission and tunneling, give a rate orders of magnitude less than that due to Eq. (5). Since $|T_{ij}|$ decreases roughly exponentially with barrier height, only the [0,3] level contributes a significant tunneling rate given by Eq. (3).

A subset of the data for interwell transition probabilities (which can be directly converted to Γ) showing these various resonances is seen in Fig. 2, where the oscillation in the RAT amplitude (the sequence of peaks running diagonally across the graph) in β_L is clearly seen. These data were obtained by varying ε at a constant rate [28] while monitoring the flux ϕ through the SQUID with a magnetometer. The change in the magnetometer output, $\Delta\phi \cong \Delta\phi_m \equiv \phi_{m1} - \phi_{m0}$ (see Fig. 1), upon a transition of fluxoid states was used to trigger a sampler, which stored the corresponding value of ε. This process was repeated 6000 times for a given β_L to obtain the transition probability histograms in Fig. 2. The focus of the remainder of this Letter is the deviation of the amplitudes of these

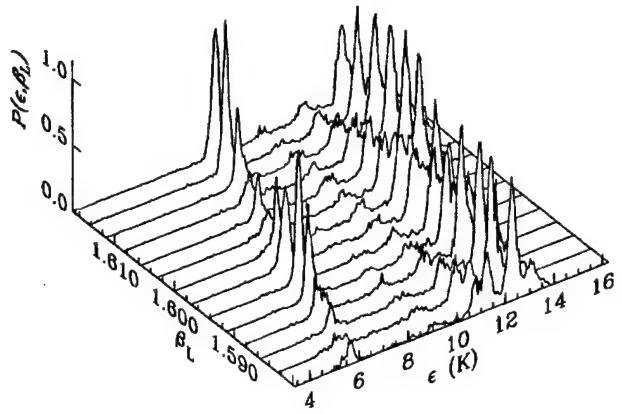

FIG. 2. The relative probabilities P for transitions from the $f = 0 \rightarrow 1$ fluxoid wells as the potential tilt ε is increased at a constant rate for a range of critical currents (β_L). The sequence of peaks running diagonally across the graph is of RAT resonances, while those roughly parallel to the β_L axis correspond to macroscopic resonant tunneling and photoinduced transition processes.

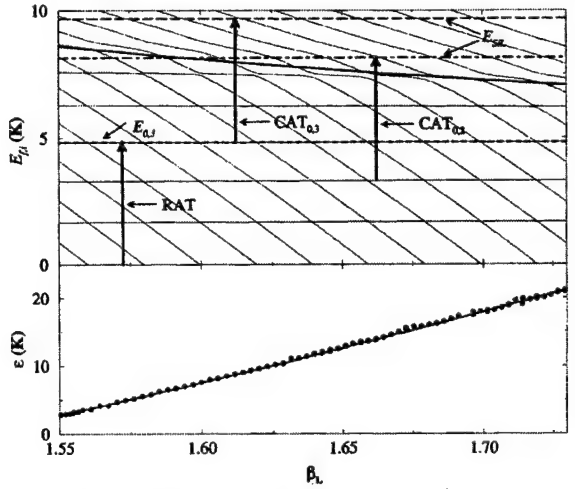

FIG. 3. Top: The calculated level structure of the system as a function of β_L for ε such that the system is on the RAT resonance ($E_{0,3} = h\nu$). The heavy arrows indicate various photon absorption processes (see text) contributing to interwell transitions. The heavy solid line shows the position of the tunnel barrier, while the intersections of the upper dashed and dash-dotted lines (E_{SIL}) with an energy level (lighter solid lines) indicate resonances due to cascaded photon absorption. Bottom: Measured (dots) vs calculated (solid line) position of peaks corresponding the RAT resonances.

RAT peaks in other regions of the parameter space from those expected on the basis of the single photon processes discussed above.

Figure 3 (top) shows the calculated level structure of the system as a function of β_L for ε such that the system is on the RAT peak. The predicted $\varepsilon(\beta_L)$ dependence for the RAT peak, along with the measured peak locations, is shown in Fig. 3 (bottom). One notes (Fig. 3), that the tunnel barrier seen from [0,3] at the RAT peak increases with decreasing β_L even though the barrier for $\varepsilon = 0$, ΔU_0, is decreasing with β_L. Since T_{ij} at the RAT peak decreases exponentially with decreasing β_L, the overall rate predicted by Eq. (3) decreases rapidly for small β_L. Figure 4 shows the measured amplitude of the RAT peaks (dots) along with those predicted considering only the single photon processes discussed above (dashed line) [29,30]. As can be seen, the agreement is very good in the large β_L, high rate, region but fails completely for small β_L. Not only are the predicted rates much lower than observed, but the locations of the predicted maxima are actually closer to those of the measured minima. This strongly suggests that, as the tunneling rate decreases, a new process is taking over as the dominant mechanism for interwell transitions.

A clue to the nature of this new process is found in the level diagram in Fig. 3 (top). Here, the dashed and dash-dotted lines indicate the energies $h\nu$ above the [0,3] and [0,2] levels, respectively. The positions of the observed maxima in the RAT amplitudes for small β_L coincide with the intersection of these energies with delocalized levels lying above the barrier, indicating that these levels serve as second intermediate levels (SIL) for the new process. The solution of the master equation including the levels up to $3h\nu$ shows that, on these resonances, the occupation of the states above [0,3] up to the second intermediate level increases significantly reaching $n_{SIL} \approx 10^{-8}$ on resonance. Since the system, once excited above the barrier, will undergo sequential decay with roughly a 50% probability of reaching the $f = 1$ well, these cascade activated transitions (CATs) involving the sequential absorption of two photons can easily give a rate much greater than that

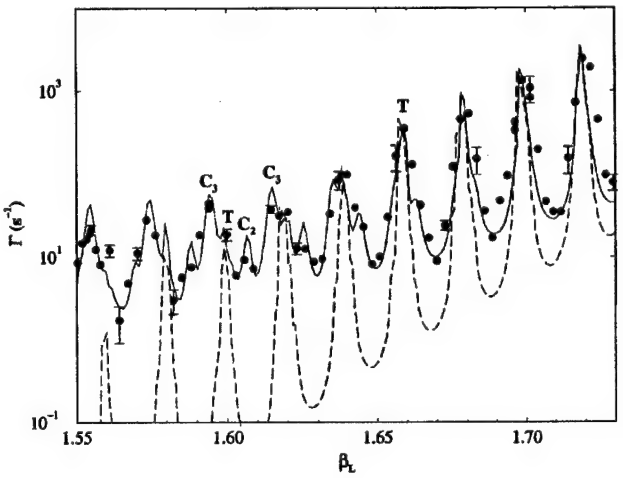

FIG. 4. Measured amplitude of the RAT resonance peaks (dots) with representative error bars compared with the calculated amplitudes including only single photon absorption (dashed line) and cascaded two-photon absorption (solid line). Several of the calculated peaks are identified with their corresponding processes by T (tunneling from [0,3]) or C (cascaded two-photon absorptions to a second resonant level above the barrier).

produced by Eq. (3) in the small β_L region. The solid curve in Fig. 4 shows the calculated transition rate including these CAT transitions (again with Gaussian smearing). Indexing the CAT processes by the initial state for the second photon absorption, the calculations show significant peaks for $CAT_{0,3}$ and $CAT_{0,2}$. The peaks in this calculated rate are labeled T (for single photon tunneling transitions—RAT) and C_3 and C_2 for the $CAT_{0,3}$ and $CAT_{0,2}$ cascade transitions, respectively. The second intermediate level for the $CAT_{0,1}$ transition lies below the barrier, and so does not give a significant transition rate. Also, the second intermediate level for the $CAT_{0,2}$ transition drops below the barrier for $\beta_L < 1.59$ (see Fig. 3), accounting for the rapid decrease in the amplitude of this peak relative to the $CAT_{0,3}$ peak for the smallest β_L. As can be seen, the data agree within experimental error with these calculated rates including cascaded two-photon processes, in marked contrast to the evident deviation from the predictions including only single photon absorption.

The calculated rates depend on two unknown parameters, the damping R and the rf flux amplitude ϕ_{xrf}. These have been used as fitting parameters with optimum values of $R = 5R_Q$ and $\phi_{xrf} = 0.001$. We estimate the uncertainty in these parameters to be about $\pm 50\%$. This value for the damping compares favorably with the value of $R = 5.3R_Q$ corresponding to the Lorentzian linewidth obtained from the deconvolution of one of the strongest RAT peaks (near $\beta_L = 1.70$) into its Lorentzian (intrinsic) and Gaussian (measurement noise) components [24]. This corresponds to a damping $\alpha \equiv \Delta\phi_m^2 \frac{R_Q}{R}$ of 0.03 putting the system well within the regime ($\alpha < 0.5$) where macroscopic quantum coherence (MQC) is possible.

In conclusion, we have observed anomalies in the transition rates between the fluxoid states of SQUIDs in microwave magnetic fields occurring when the parameters ε and β_L of the potential are such that a state within the initial well is resonant with the microwave photons. The transition rates measured at the resonant peaks (RAT) corresponding to these conditions agree well with those calculated including cascaded two-photon absorption by the system. In particular, for low critical current (β_L), where tunneling involving single photon absorption is suppressed, the measured peak amplitudes show local maxima where a second intermediate level has an energy $h\nu$ above the initial resonant level. These data provide the first confirmation of such two-photon transitions in SQUIDs, and indicate the importance of considering these processes as potential sources of decoherence in SQUID qubits.

The authors are grateful for many helpful discussions with D. Averin, A. Garg, and K. Likharev. This work was supported in part by AFOSR No. F49620-99-1-0205, the State of Kansas No. S99041, and NSF No. DMR9876874 (Kansas), and by NSF No. DMR9876850 and ARO No. DAAD19-99-1-0341 (Stony Brook).

[1] E. Schrödinger, Naturwissenschaften **23**, 844 (1935).
[2] A. Leggett, Contemp. Phys. **25**, 583 (1984).
[3] A. Leggett and A. Garg, Phys. Rev. Lett. **54**, 857 (1985).
[4] L. Ballentine, Phys. Rev. Lett. **59**, 1493 (1987).
[5] A. Caldeira and A. Leggett, Phys. Rev. Lett. **46**, 211 (1981).
[6] S. Chakravarty, Phys. Rev. Lett. **49**, 681 (1982).
[7] S. Chakravarty and S. Kivelson, Phys. Rev. Lett. **50**, 1811 (1983).
[8] S. Chakravarty and A. J. Leggett, Phys. Rev. Lett. **52**, 5 (1984).
[9] M. P. Fisher and A. Dorsey, Phys. Rev. Lett. **54**, 1609 (1985).
[10] A. Leggett *et al.*, Rev. Mod. Phys. **59**, 1 (1987).
[11] W. Zwerger, Z. Phys. B **53**, (1983).
[12] U. Weiss, H. Grabert, and S. Linkwitz, J. Low Temp. Phys. **68**, 213 (1987).
[13] E. Chudnovsky and L. Gunther, Phys. Rev. Lett. **60**, 661 (1988).
[14] R. F. Voss and R. A. Webb, Phys. Rev. Lett. **47**, 265 (1981).
[15] S. Washburn, R. Webb, R. Voss, and S. Faris, Phys. Rev. Lett. **54**, 2712 (1985).
[16] J. M. Martinis, M. H. Devoret, and J. Clarke, Phys. Rev. Lett. **55**, 1543 (1985).
[17] D. Schwartz, B. Sen, C. Archie, and J. Lukens, Phys. Rev. Lett. **55**, 1547 (1985).
[18] M. H. Devoret, J. M. Martinis, and J. Clarke, Phys. Rev. Lett. **55**, 1908 (1985).
[19] S. Han, J. Lapointe, and J. Lukens, Phys. Rev. Lett. **66**, 810 (1991).
[20] R. Rouse, S. Han, and J. Lukens, Phys. Rev. Lett. **75**, 1614 (1995).
[21] S. Han, R. Rouse, and J. Lukens, Phys. Rev. Lett. **76**, 3404 (1996).
[22] P. Silvestrini, V. Palmieri, B. Ruggiero, and M. Russo, Phys. Rev. Lett. **79**, 3046 (1997).
[23] S. Lloyd, Science **261**, 1569 (1993).
[24] R. Rouse, S. Han, and J. Lukens, in *Phenomenology of Unification from Present to Future,* edited by G. D. Palazzi, C. Cosmelli, and L. Zanello (World Scientific, Singapore, 1998), pp. 207–224.
[25] W. Bialek, S. Chakravarty, and S. Kivelson, Phys. Rev. B **35**, 120 (1987).
[26] J. Schmidt, A. Cleland, and J. Clarke, Phys. Rev. B **43**, 229 (1991).
[27] A delocalization also occurs for values of ε such that $E_{0,i} = E_{1,j}$. However, this effect is not important for the results presented here, since it occurs for a range of ε much less than the instrumental smearing of ε, as discussed in the text.
[28] The rate of change of Φ was always sufficiently slow ($<1\Phi_0\ s^{-1}$) that the sample is well into the adiabatic regime.
[29] Note that the photon-induced transition process is included in this theory curve but contributes a maximum of 10% (and usually much less) to these amplitudes.
[30] These calculated rates include a Gaussian smearing with FWHM of 2×10^{-4} in ϕ_x to account for the measured effect of the magnetometer noise on the trigger circuit, which samples ϕ_x when a fluxoid transition occurs.

Appendix B

INSTITUTE OF PHYSICS PUBLISHING SUPERCONDUCTOR SCIENCE AND TECHNOLOGY
Supercond. Sci. Technol. 15 (2002) 1–4 PII: S0953-2048(02)27352-2

Observation of temporal evolution of an unstable macroscopic quantum system with nanoseconds resolution

Yang Yu[1], Yu Zhang[1], Wei Qiu[1], Shaoxiong Li[1], Siyuan Han[1] and Zhen Wang[2]

[1] Department of Physics and Astronomy, University of Kansas, Lawrence, KS 66045, USA
[2] Kansai Advance Research Center, Communication Research Laboratory, Ministry of Posts and Telecommunications, 588-2 Iwaoka, Iwaoka-cho, Nishi-Ku, Kobe, 651-24 Japan

Received 26 July 2001, in final form 15 October 2001
Published DD MMM 2002
Online at stacks.iop.org/SUST/15/1

Abstract
High-resolution (sub-microsecond to nanosecond) time-resolved measurements of the dynamics of superconducting electronic devices, such as Josephson tunnel junctions and SQUIDs, are indispensable for fundamental physics research, such as quantum mechanics of macroscopic variables. We describe the development of a time-resolved measurement technique that enables direct measurements, in the time domain, of the temporal evolution of Josephson junctions with nanosecond resolution. The technique was applied to study escape dynamics of Josephson junctions, as macroscopic quantum systems, in the quantum tunnelling regime. The measured probability of junctions remaining in the initial metastable state—the survival probability—as a function of time decayed exponentially, agreeing very well with the theoretical prediction of the incoherent tunnelling process.

1. Introduction

Quantum mechanics at the macroscopic level and the physical realization of quantum computing present two of the biggest challenges to scientists and engineers around the world. Since early 1980s, Josephson junctions and SQUIDs have proven to be excellent systems for both the theoretical and experimental study of the quantum mechanics of macroscopic variables due to their simple structure and high degree of characterization [1–6]. For instance, experiments showed some remarkable macroscopic quantum effects, such as macroscopic quantum tunnelling (MQT) through a barrier [4, 7, 8], energy level quantization within a well [9–11], macroscopic resonant tunnelling and photon-assisted tunnelling [10, 12], and photon-induced transition and population inversion between macroscopically distinct states [13, 14]. Recently, the quantum superposition of two macroscopic states has been observed by measuring the energy spectra of fluxiod states in SQUIDs [15, 16]. However, due to the lack of a high-resolution time-resolved measurement scheme, coherent oscillations between two macroscopically distinct states in the time domain, which would be the most direct demonstration of microscopic quantum coherence (MQC), remains unobserved. On the other hand, as a fruit of these basic researches and the development of Josephson junction-based superconducting integrated circuit technology, superconducting electronic devices, such as various SQUIDs and single-pair tunnelling devices, are recognized as promising candidates for the solid-state qubits [17, 18]. Since most of the proposed quantum logic operations, e.g. Hadamard transform and controlled-NOT gate, propagate the quantum state of qubits in time, it is imperative to be able to monitor the temporal evolution of Josephson devices with resolution comparable to the typical gate time of 1–10 ns. In this paper, we describe the development of a time-resolved measurement technique for Josephson devices that allowed us to investigate, for the first time, the time-dependent tunnelling probability $P_{MQT}(t)$ of a macroscopic system. The results demonstrate that our time-resolved measurement has achieved nanosecond resolution. The measured $P_{MQT}(t)$ showed excellent exponential time dependence, characteristic of incoherent tunnelling.

0953-2048/02/000001+04$30.00

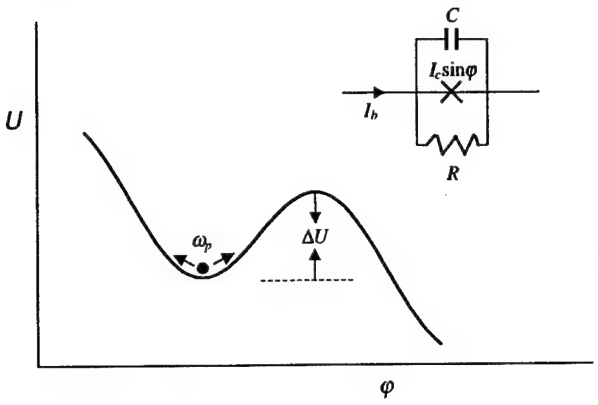

Figure 1. Potential energy of a Josephson junction biased below critical current. Inset shows the electrical equivalent circuit of a current biased junction.

2. Experiment

2.1. Principles and procedures

In our experiment, we studied the tunnelling probability of current-biased Josephson junctions as a function of time. A current-biased Josephson tunnel junction with critical current I_c, can be modelled as a 'phase' particle moving in a one-dimensional washboard potential $U(\varphi) = -i_b\varphi - E_J \cos\varphi$ with a friction coefficient proportional to R^{-1}. Here, the particle's mass is proportional to the junction capacitance C, $E_J \equiv I_c\Phi_0/2\pi$ is the Josephson coupling energy, $\Phi_0 = h/2e$ is flux quantum, $i_b \equiv I_b/I_c$ is the bias current normalized to I_c, φ is the phase difference across the junction that represents the position of the particle, and R is the junction's shunt resistance. For $i_b < 1$, the potential has metastable wells separated by barriers ΔU (figure 1). The barrier height is given by $\Delta U = 2E_J\left[\left(1-i_b^2\right)^{1/2} - i_b\cos^{-1} i_b\right]$. The dc voltage across the junction corresponds to the particle's average velocity that is zero when the particle is trapped in a potential well and is finite when it is running down the washboard potential. At the bottom of the well, the particle oscillates with the plasma frequency $\omega_p \equiv \omega_{p0}\left(1-i_b^2\right)^{1/4}$, where $\omega_{p0} \equiv (2\pi I_c/C\Phi_0)^{1/2}$. ΔU is a decreasing function of the bias current i_b and becomes zero for $i_b \geqslant 1$. At low temperatures, $T = h\omega_p/2\pi k_B$, the particle can escape from a potential well via quantum tunnelling. For a junction prepared in the zero-voltage state at $t = 0$, the probability of finding the junction remaining in this state, also called survival probability $P_s(t)$, decays exponentially with a time constant (i.e. lifetime) $\tau \equiv \Gamma_t^{-1}$

$$P_s(t) = \mathrm{e}^{-t/\tau} \tag{1}$$

where Γ_t is the tunnelling rate which depends on ΔU, $h\omega_p$, R and T. Therefore, the tunnelling probability is given by

$$P_{\mathrm{MQT}}(t) = 1 - P_s(t) \tag{2}$$

To obtain time-dependent survival probability at a constant bias current, we start a measurement cycle by increasing the bias current, which was generated by a 12-bit waveform generator connected to a PC via GPIB interface (figure 2), to a desired level. The bias current was kept constant

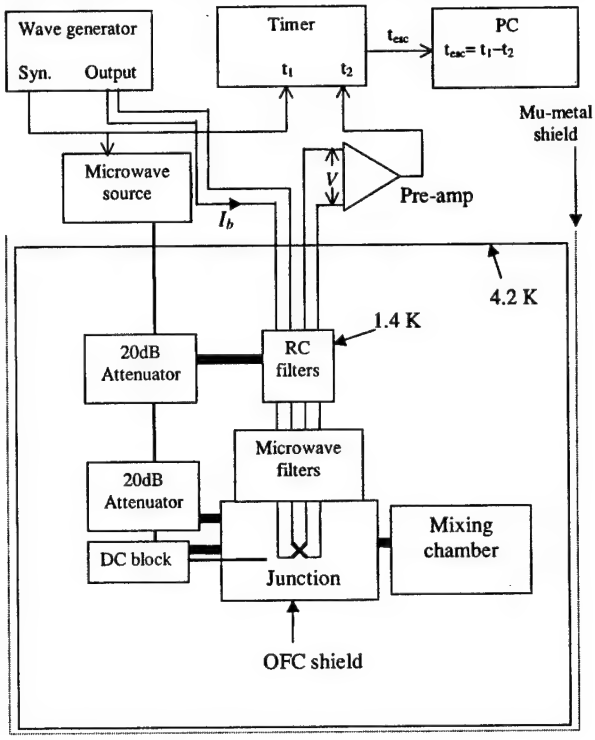

Figure 2. Schematic of the experimental set-up.

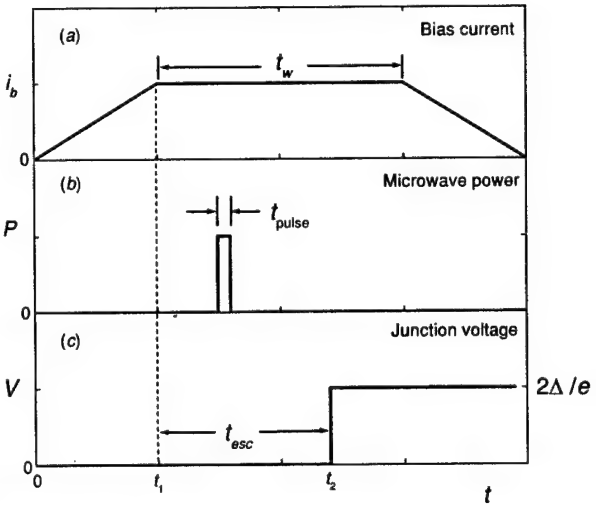

Figure 3. Timing sequence of (*a*) the junction bias current, (*b*) the microwave power, and (*c*) the junction's voltage response.

for a period of t_w, called 'waiting time,' before being decreased to zero (figure 3). The voltage across the junction was sent to a HP33250 universal counter/timer that was set for time interval measurement. The first and second channels of the timer were triggered by the waveform generator's sync output and the junction voltage to record t_1 (the initial time) and t_2 (the time when tunnelling occurred). Hence, the escape time is given by $t_{\mathrm{esc}} = t_2 - t_1$. For a given bias current and waiting time this process was repeated $\sim 10^4$ times. The value of $P_{\mathrm{MQT}}(t)$ at a time t' was obtained by calculating the fraction of all tunnelling events that occurred before t'.

As the tunnelling rate depends exponentially on $\Delta U/\hbar\omega_p$ so the time constant of the decaying survival probability can be varied over several orders of magnitude by changing the bias current level. Hence, the time resolution of this measurement technique can be determined *in situ* by stepping up the bias current level.

2.2. *Samples and set-up*

For data presented in this study, we used NbN/AlN/NbN tunnel junctions fabricated on a single crystal MgO substrate [19, 20]. The junctions were of high quality, with a sharp rise in the quasiparticle tunnelling current at $2\Delta/e$, a low subgap leakage current, and a quite uniform critical current density J_c. The critical temperature T_c of the junction was about 16 K. In order to have low dissipation, junctions with low critical current density were chosen. Data reported below were taken from the largest junction (10×10 μm^2) on the chip so that parasitic capacitance of the leads had negligible effect on the junction's dynamics. Switching current distribution [21] and resonant activation measurements [5] at 4.2 K were performed to determine the most important junction parameters I_c and C. These measurements gave $I_c = 156.86$ μA and $C = 5.8 \pm 0.6$ pF, respectively. I_c stayed essentially constant below 4.2 K due to the NbN tunnel junction's large gap energy ($\Delta = 2.7$meV). The sample was mounted on a chip carrier that was enclosed in a helium-filled oxygen-free copper sample cell. The sample cell was thermally anchored to the mixing chamber of an Oxford Kelvinox 400 dilution refrigerator (figure 2). The junction was magnetically shielded by a μ-
Q1 metal cylinder surrounded by the cryostat. All electrical leads that connected the junction to room temperature electronics were carefully filtered by EMI filters (at ~300 K), RC filters (at ~1.4 K) and microwave filters (at mixing chamber temperature) [22]. Battery-powered low-noise pre-amplifiers were used for all measurements. Care was taken to eliminate ground loops in the set-up. For instance, optically coupled isolation amplifiers were used to break direct connections between the battery-powered and ac-powered parts of the set-up. The measured junction voltage noise spectrum showed no peak at 60 Hz and its harmonics, confirming the good quality of our experimental set-up. Microwave pulses could be injected via a separate coaxial cable, with 40 dB attenuation inside the cryostat, that was capacitively coupled to the junction.

2.3. *Time-domain observation of incoherent tunnelling*

Although incoherent tunnelling between two macroscopic distinct states of a SQUID had been observed about a decade ago [23], the measurement was carried out in the frequency domain. Here, we report results obtained from time-domain measurements which clearly demonstrate the incoherent nature of the tunnelling process in a Josephson junction biased at constant currents. Figure 4 shows the measured temporal survival probability functions at several bias current levels. The data were taken at 20 mK, well below the classical-to-quantum crossover temperature, where the junction escape from the well by MQT. From the semi-log plot of figure 4 it is clear that $P_s(t)$ decays exponentially and that the lifetime τ decreased as the barrier height is reduced.

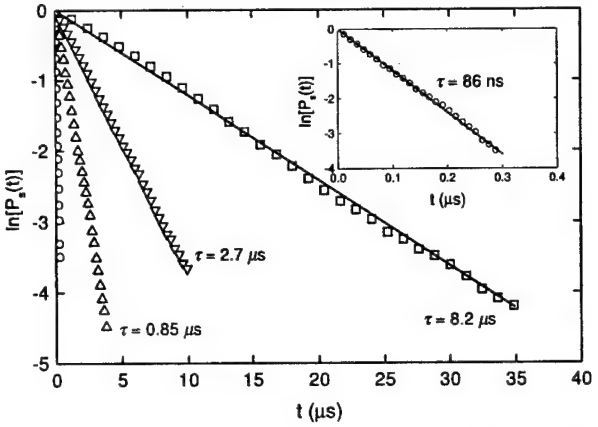

Figure 4. The measured time-dependent survival probabilities $P_s(t)$ versus time. The data were taken at $T = 20$ mK. From the left to right: the bias currents were 150.75 μA, 150.28 μA, 150.09 μA and 149.95 μA. Symbols are data (with one out of five points shown for clarity) and the solid straight line is fit. Inset is a magnified view of the data taken at $I_b = 150.75$ μA.

It is worth noting that using this time-domain method we are able to measure tunnelling rate in the Josephson junctions between about 10 s^{-1} and 2×10^7s^{-1}, a range over six orders of magnitude, with very good accuracy. While the capability of measuring higher rates was limited by time resolution of the instruments and signal-to-noise ratio in junction voltage detection circuit, there was no fundamental limitation to measuring lower rates other than the available experimental time. By contrast, the traditional method of rate measurements (by ramping bias current up continuously until the junction escapes) usually can only cover a four-decade range with adequate accuracy [5, 21]. Hence, our method also provides a powerful tool for the study of escape dynamics in junctions with very low barrier, a regime that was not accessible by the traditional method before. The inset of figure 4 also demonstrate that our time domain technique has achieved nanosecond resolution.

2.4. *The effect of microwave pulse*

In addition to tunnelling from the ground level of a potential well, a microwave pulse can be applied to the junction to create a significant population at the excited levels. The energy barrier for tunnelling from an excited level $|n\rangle$ is lowered by an amount of E_n, where E_n is the excited level's energy with respect to the ground level. Therefore, the tunnelling rate could be substantially increased when a microwave is applied to the junction. A better way to observe the microwave-induced enhancement of tunnelling rate is to apply a short microwave pulse to the junction in each measurement cycle (figure 3(b)). Here, 'short' means that the duration of the microwave pulse $t_{\rm pulse} = \tau$, where τ is the lifetime without microwave irradiation. The time resolution of our time-domain measurement system can also be verified by decreasing $t_{\rm pulse}$, while keeping the frequency and power of the microwave pulse constant, until its effect could not be discerned anymore. Figure 5 shows the data taken with one microwave pulse of 100 ns duration per cycle at $T = 20$ mK. The effect of tunnelling rate enhancement by the microwave pulse is

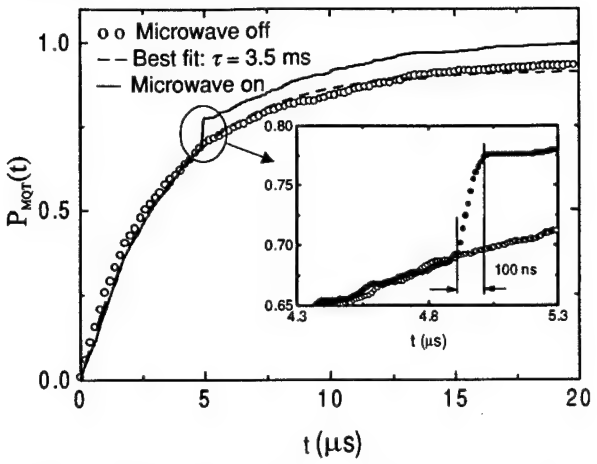

Figure 5. Time-dependent tunnelling probability, $1 - P_s(t)$, with one microwave pulse (solid line) and without microwave (open circles). The dashed line is the best fit to equation (2). Inset shows the detail in the vicinity of the microwave pulse, where the solid dots are data taken with the microwave pulses.

clearly demonstrated. In this experiment, our goal is simply to observe a strong effect of microwave pulse on the tunnelling rate. Therefore, the frequency of the microwave was not tuned to the energy level spacing of the junction and the power used was rather high (about −70 dBm before entering the sample cell).

3. Summary

We have developed a measurement technique capable of monitoring the temporal evolution of metastable (or bistable) Josephson junction-based macroscopic quantum systems with nanosecond resolution. The resolution of the method was demonstrated by tunnelling rate measurement in junctions with very low barrier (thereby very short lifetime) and by observing the microwave-enhanced tunnelling with sub-μs pulses. The method was applied to obtain time-dependent survival probability $P_s(t)$ of the Josephson junctions initially prepared in the zero-voltage state. The observation of exponentially decaying $P_s(t)$ reveals the incoherent nature of the tunnelling process. The method is suitable for the study of temporal behaviour of Josephson junctions with lifetime between about 50 ns and 0.1 s.

Acknowledgments

The authors thank Prof Shih-I Chu for useful discussions. This study is supported in part by NSF no DMR-9876874 and no EIA-0082499, AFOSR no F49620-99-1-0205, and the State of Kansas no S99041.

References

[1] Caldeira A O and Leggett A J 1981 Influence of dissipation on quantum tunneling in macroscopic systems *Phys. Rev. Lett.* **46** 211

[2] Leggett A J, Chakravarty S, Dorsey A T, Fisher M P A, Garg A and Zwerger W 1987 Dynamics of the dissipative two-state system *Rev. Mod. Phys.* **59** 1

[3] Grabert H, Weiss U and Hanggi P 1984 Quantum tunneling in dissipative systems at finite temperatures *Phys. Rev. Lett.* **52** 2193

[4] Washburn S, Webb R A, Voss R F and Faris S M 1985 Effects of dissipation and temperature on macroscopic quantum tunneling *Phys. Rev. Lett.* **54** 2712

[5] Clarke J, Cleland A N, Devoret M H, Esteve D and Martinis J M 1988 Quantum mechanics of a macroscopic variable: the phase difference of a Josephson junction *Science* **239** 992

[6] Rouse R, Han S and Lukens J E 1998 Resonant tunneling between macroscopically distinct levels of a SQUID *Phenomenology of Unification from Present to Future* ed G Diambrini Palazzi *et al* (Singapore: World Scientific) p 207

[7] Devoret M H, Martinis J M and Clarke J 1985 Measurements of macroscopic quantum tunneling out of the zero-voltage state of a current-biased Josephson junction *Phys. Rev. Lett.* **55** 1908

[8] Schwartz D B, Sen B, Archie C N and Lukens J E 1985 Quantitative study of the effect of the environment on macroscopic quantum tunneling *Phys. Rev. Lett.* **55** 1547

[9] Martinis J M, Devoret M H and Clarke J 1985 Energy-level quantization in the zero-voltage state of a current biased Josephson junction *Phys. Rev. Lett.* **55** 1543

[10] Rouse R, Han S and Lukens J E 1995 Observation of resonant tunneling between macroscopically distinct quantum levels *Phys. Rev. Lett.* **75** 1614

[11] Silvestrini P, Palmieri V G, Ruggiero B and Russo M 1997 Observation of energy-level quantization in underdamped Josephson junctions above the classical-quantum regime crossover temperature *Phys. Rev. Lett.* **79** 3046

[12] Rouse R, Han S and Lukens J E 1996 Photon assisted resonant tunneling between macroscopically distinct quantum states of a SQUID *Quantum Coherence and Decoherence* ed K Fujikawa and Y Ono (Amsterdam: Elsevier) p 179

[13] Han S, Rouse R and Lukens J E 2000 Observation of cascade two-photon-induced transitions between fluxoid states of a SQUID *Phys. Rev. Lett.* **84** 1300

[14] Han S, Rouse R and Lukens J E 1996 Generation of a population inversion between quantum states of a macroscopic variable *Phys. Rev. Lett.* **76** 3404

[15] Friedman J R, Patel V, Chen W, Tolpygo S K and Lukens J E 2000 Quantum superposition of distinct macroscopic states *Nature* **406**

[16] van der Wal C H, Haar ter A C J, Wilhelm F K, Schouten R N, Harmans C J P M, Orlando T P, Seth Lloyd and Mooij J E 2000 Quantum superposition of macroscopic persistent-current states *Science* **290** 773

[17] Orlando T P, Mooij J E, Tian Lin, van der Wal C H, Levitov L S, Lloyd S and Mazo J J 1999 Superconducting persistent-current qubit *Phys. Rev.* B **60** 15398

[18] Shnirman A, Schon G and Hermon Z 1997 Quantum manipulation of small josephson junctions *Phys. Rev. Lett.* **79** 2371

[19] Wang Z, Kawakami A, Uzawa Y and Komiyama B 1995 NbN/AlN/NbN tunnel junctions fabricated at ambient substrate temperature *IEEE Trans. Appl. Supercond.* **5** 2322

[20] Wang Z, Kawakami A and Uzawa Y 1997 NbN/AlN/NbN tunnel junctions with high current density up to 54 kA/cm^2 *Appl. Phys. Lett.* **70** 114

[21] Jackel L D, Webb W W, Lukens J E and Pei S S 1974 Measurement of the probability distribution of thermally excited fluxoid quantum transitions in a superconducting ring closed by a Josephson junction *Phys. Rev.* B **9** 115

[22] Zorin A B 1995 The thermocoax cable as the microwave frequency filter for single electron circuits *Rev. Sci. Instrum.* **66** 4296

[23] Han S, Lapointe J and Lukens J E 1991 Observation of incoherent relaxation by tunneling in a macroscopic two-state system *Phys. Rev. Lett.* **66** 810

Queries

(1) Author: Please check the change in sentence 'The junction was . . . '

Appendix C

References and Notes

1. T. Someya, H. Akiyama, H. Sakaki, *Phys. Rev. Lett.* **74**, 3664 (1995).
2. F. Vouilloz *et al.*, *Phys. Rev. B* **57**, 12378 (1998).
3. H. Akiyama, T. Someya, H. Sakaki, *Phys. Rev. B* **53**, R4229 (1996).
4. P. Ils *et al.*, *Phys. Rev. B* **51**, 4272 (1995).
5. J. Hasen *et al.*, *Nature* **390**, 54 (1997).
6. X. Duan, C. M. Lieber, *Adv. Mater.* **12**, 298 (2000).
7. M. S. Gudiksen, C. M. Lieber, *J. Am. Chem. Soc.* **122**, 8801 (2000).
8. M. S. Gudiksen, J. Wang, C. M. Lieber, *J. Phys. Chem. B* **105**, 4062 (2001).
9. Excitation light (488 or 514 nm) was focused by an objective (NA = 0.7) to a ~30-μm diameter spot at ~1.0 kW/cm² on the quartz substrate with nanowires dispersed on it. A λ/2 wave plate was used to change the polarization of excitation light. The resulting PL was collected by the same objective, filtered to remove excitation light, focused, and either imaged or spectrally dispersed onto a liquid nitrogen–cooled CCD. To determine the emission polarization, a Glan-Thompson polarizer was placed in front of the spectrometer to detect emission intensities.
10. S. A. Empedocles, D. J. Norris, M. G. Bawendi, *Phys. Rev. Lett.* **77**, 3873 (1996).
11. PL spectra exhibit a diameter-dependent shift in the PL emission energy from the bulk band gap of InP (1.35 eV) for diameters ≤20 nm. Detailed studies show that diameter-dependent spectra collected from nanowires at room temperature and ~7 K can be explained in terms of radial quantum confinement. Giant polarization anisotropy is observed in nanowires with diameters from 10 to 50 nm at room temperature and 7 K.
12. M. S. Gudiksen, J. Wang, C. M. Lieber, in preparation.
13. L. D. Landau, E. M. Lifshitz, L. P. Pitaevskii, *Electrodynamics of Continuous Media* (Pergamon, Oxford, 1984), pp. 34–42.
14. X. Duan, Y. Huang, Y. Cui, J. Wang, C. M. Lieber, *Nature* **409**, 66 (2001).
15. Y. Huang, X. Duan, Q. Wei, C. M. Lieber, *Science* **291**, 630 (2001).
16. Y. Cui, C. M. Lieber, *Science* **291**, 851 (2001).
17. S. Ura, H. Sunagawa, T. Suhara, H. Nishihara, *J. Lightwave Tech.* **6**, 1028 (1988).
18. C. J. Chen, K. K. Choi, L. Rokhinson, W. H. Chang, D. C. Tsui, *Appl. Phys. Lett.* **74**, 862 (1999).
19. M. Bass *et al.*, *Handbook of Optics* (McGraw Hill, New York, 1995), pp. 17.1–17.29.
20. These very small devices could prove useful for high-speed detection because the response times of semiconductor photodetectors can be limited by their resistance-capacitance (RC) time constants (*19*). On the basis of improved nanowire–metal contacts (10 kilohm) and intrinsically small capacitances (~10^{-17} F) (*21*), RC time constants on the order of 100 fs can be realized. By decreasing the electrode separation to ensure direct collection of photogenerated carriers, detection speeds on the order of 100 fs or less may be realized with these nanoscale detectors.
21. Y. Cui, X. Duan, J. Hu, C. M. Lieber, *J. Phys. Chem. B* **104**, 5213 (2000).

22. We thank L. Lauhon and H. Park for helpful discussions. M.S.G. thanks the NSF for predoctoral fellowship support. C.M.L. acknowledges support of this work by the Office of Naval Research and Defense Advanced Projects Research Agency.

8 May 2001; accepted 24 August 2001

Time-Resolved Measurement of Dissipation-Induced Decoherence in a Josephson Junction

Siyuan Han,[1]* Yang Yu,[1] Xi Chu,[2] Shih-I Chu,[2] Zhen Wang[3]

We determined the dissipation-induced decoherence time (DIDT) of a superconducting Josephson tunnel junction by time-resolved measurements of its escape dynamics. Double-exponential behavior of the time-dependent escape probability was observed, suggesting the occurrence of a two-level decay-tunneling process in which energy relaxation from the excited to the ground level significantly affects the escape dynamics of the system. The observation of temporal double-exponential dependence enables direct measurements of the DIDT, a property critical to the study of quantum dynamics and the realization of macroscopic quantum coherence and quantum computing. We found that the DIDT was $\tau_d > 11$ μs at $T = 0.55$ K, demonstrating good prospects for implementing quantum computing with Josephson devices.

Use of solid-state devices (SSD) is regarded as one of the most promising approaches for the development of quantum computers (QC), due to the relative ease of circuit design, fabrication, and scaling up (*1–10*). However, coupling between SSD and the environment results in dissipation, and hence decoherence. Here, decoherence refers to processes that lead to exponential decay of superposition states into incoherent mixtures. The severity of decoherence is characterized by the decoherence time—the time constant τ of the exponential decay. Both dissipation (with decoherence time τ_d) and phase relaxation (with τ_φ) lead to decoherence (*11–15*). Realization of QC will depend critically on our ability to create and preserve coherent superposition states so that decoherence presents the most fundamental obstacle (*11–16*). One way to increase the decoherence time in SSD is to use superconducting qubits (SQ) based on superconducting quantum interference devices (SQUIDs) (flux qubits) or single-pair tunneling devices (charge qubits) (*3–10*). For both types of SQ, the Josephson junction is the key element and it is the dissipation of the junctions that will set the limit on decoherence time. Furthermore, for SQUID qubits τ_d^{-1} and τ_φ^{-1} are predicted to be proportional to the level of dissipation (*17, 18*). Therefore, the feasibility of implementing QC with SQ depends on whether dissipation in Josephson junctions can be made sufficiently low to keep the error rate to a tolerable level. However, experimental determination of either τ_d or τ_φ is extremely difficult for superconducting devices because in each measurement only a single device, rather than an ensemble of identical devices, is available for signal detection. Furthermore, prior to this work no time-domain measurement with resolution comparable to the decoherence time scale of SQ has been demonstrated. For these reasons, no time-resolved measurement of τ_d (or τ_φ) has been reported yet. Recent attempts to determine the effective damping resistance of a Josephson junction in a SQUID were inconclusive due to the questionable method of data analysis used and the indirect nature of the measurement technique (*19, 20*). We present time-resolved measurements of τ_d in a NbN/AlN/NbN Josephson junction. The measured decoherence time, $\tau_d > 10$ μs at $T = 0.55$ K, corresponds to a qubit quality factor $\tau_d/\tau_{op} \sim 10^4$ (where $\tau_{op} \sim 1$ ns is the typical gate time of SQUID qubits), demonstrating strong potential for QC employing NbN SQUID qubits (*12*).

The equation of motion for a current biased Josephson junction, $Cd^2\Phi/dt^2 + R^{-1}d\Phi/dt = -\partial U/\partial\Phi$, is homologous to that of a particle of mass C moving in a washboard potential $U(\Phi) = -I_b\Phi - E_J\cos(2\pi\Phi/\Phi_0)$ with damping constant R^{-1}, where C is the junction capacitance, R is the shunt resistance, $\Phi_0 \equiv h/2e$ is the flux quantum, $E_J \equiv I_c\Phi_0/2\pi$ is the magnitude of maximum Josephson coupling energy, I_c is the critical current of the junction, I_b is the bias current, and $\Phi \equiv (\varphi/2\pi)\Phi_0$, where φ is the phase difference across the junction. For $i_b \equiv I_b/I_c < 1$, the potential has a series of metastable wells. The dc voltage across the junction is zero when the particle is trapped in a potential well. The depth of the potential well decreases as i_b is increased and becomes zero for $i_b \geq 1$. In the presence of thermal/quantum fluctuations, a junction initially trapped in the zero-voltage state can escape from the potential well to enter the finite-voltage state.

Previous experiments have demonstrated

[1]Department of Physics and Astronomy, University of Kansas, Lawrence, KS 66045, USA. [2]Department of Chemistry, University of Kansas, Lawrence, KS 66045, USA. [3]Kansai Advanced Research Center, Communication Research Laboratory, Ministry of Posts and Telecommunications, 588-2 Iwaoka, Iwaoka-cho, Nishi-ku, Kobe, 651-24 Japan.

*To whom correspondence should be addressed. E-mail: han@ku.edu

that when damping is sufficiently low the junction is a macroscopic quantum object with quantized energy levels (*21, 22*). For weak damping, the quality factor of the junction is $Q \equiv \omega_p RC$, where $\omega_p = (2\pi I_c/C\Phi_0)^{1/2}(1 - i_b^2)^{1/4}$ is the plasma frequency of the junction. The primary effect of weak damping ($Q \gg 1$) on the intrawell dynamics of the junction is that at low temperature ($k_B T \ll$ level separation) the width of an excited level $|n\rangle$, with energy E_n, is given approximately by $\delta E_n \simeq E_n/Q$ (*23, 24*). In thermal equilibrium, escape from the potential well is dominated by macroscopic quantum tunneling (MQT) from the ground level $|0\rangle$ for $T \ll \hbar\omega_p/k_B$. By contrast, in a nonequilibrium state the excited levels could have excessive population that can be created by rapidly ramping up the bias current and/or applying dc pulse or microwave excitations. For nonequilibrium states, tunneling from excited levels can be important to the escape process. In particular, tunneling from overpopulated excited levels can dominate the escape process even at temperatures much higher than the crossover temperature for the ground state MQT, as demonstrated by recent experiments (*25*).

At low temperatures, the simplest nonequilibrium escape process that involves tunneling from both the ground and the excited levels is the two-level decay-tunneling (TLDT) process (Fig. 1), which allows a direct measurement of τ_d. For a junction with probability $\rho_{11}(0)$ in the level $|1\rangle$ at $t = 0$, the probability of finding it remaining in the zero-voltage state at $t > 0$ is given by

$$P(t) = (1 - \gamma)e^{-\Gamma_0 t} + \gamma e^{-\Gamma' t} \qquad (1)$$

where $\Gamma' \equiv \Gamma_1 + \Gamma_d$, $\Gamma_0(\Gamma_1)$ is the escape rate from the level $|0\rangle$ ($|1\rangle$) out of the potential well, Γ_d is the spontaneous decay rate from $|1\rangle$ to $|0\rangle$, and $\gamma \equiv \rho_{11}(0)[1 - \Gamma_d/(\Gamma' - \Gamma_0)]$ is bounded between zero and unity. The transition from $|0\rangle$ to $|1\rangle$, which is negligible at low temperature, was not included in the model.

The interlevel decay rate,

$$\Gamma_d = \frac{2\pi(E_1 - E_0)}{\hbar}\frac{R_Q}{R}|\langle 0|\phi|1\rangle|^2 \times \left[1 + \coth\left(\frac{E_1 - E_0}{2k_B T}\right)\right] \qquad (2)$$

is $\propto R^{-1}$ (*16*). Where, $E_1 - E_0$ is the energy separation between levels $|0\rangle$ and $|1\rangle$, $R_Q \equiv h/4e^2$ is the resistance quantum, and $\phi \equiv \varphi/2\pi$. For quadratic potentials $\Gamma_d \to E_1/Q$ in the limit of $k_B T \ll E_1$ as expected (*23, 24*). The ϕ matrix element and $E_1 - E_0$ can be calculated from the independently measured junction parameters so that R can be determined directly from Γ_d.

The most distinctive feature of the TLDT process is the double-exponential decay of $P(t)$ (Eq. 1). The time-dependent escape probability, $P_{esc}(t) = 1 - P(t)$, has two characteristic time scales: the average lifetimes, $\tau_0 \equiv 1/\Gamma_0$ and $\tau' \equiv 1/\Gamma'$, of the junction in levels $|0\rangle$ and $|1\rangle$, respectively. However, whether the double-exponential time dependence can be observed depends crucially on the relative magnitude of the three rate constants. Qualitatively speaking, if the junction is initially in $|1\rangle$ and $\Gamma_d \gg \Gamma_1$ (i.e., $\gamma \ll 1$) the system will decay rapidly to $|0\rangle$ before having a chance to escape from $|1\rangle$. Thus, only the slow component of the double-exponential behavior of $P_{esc}(t)$ can be observed. In the opposite limit of $\Gamma_d \ll \Gamma_1$ (i.e., $\gamma \approx 1$) the system mainly escapes from $|1\rangle$ before decaying to $|0\rangle$. Therefore, only the fast component can be observed. Because junction resistance increases as temperature is lowered, one expects the former (latter) behavior at high (low) temperatures. The situation is quite different for the intermediate temperature regime where Γ_d is comparable to Γ_1 (i.e., $\gamma \approx 0.5$). In this case, the probabilities of escaping out of the zero-voltage state from either $|0\rangle$ or $|1\rangle$ are approximately equal and the double-exponential behavior should be observed clearly, from which three parameters, γ, Γ_0, and Γ', can be extracted directly from the measured $P_{esc}(t)$. Although τ_d cannot be determined exactly from $P_{esc}(t)$ measurement due to the incomplete knowledge about $\rho_{11}(0)$, its lower bound is set by $1/\Gamma'$ since $\Gamma' > \Gamma_d$.

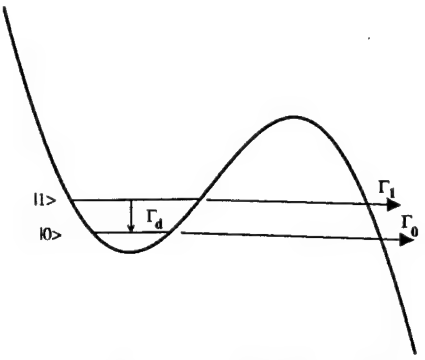

Fig. 1. Illustration of the TLDT process described in the text.

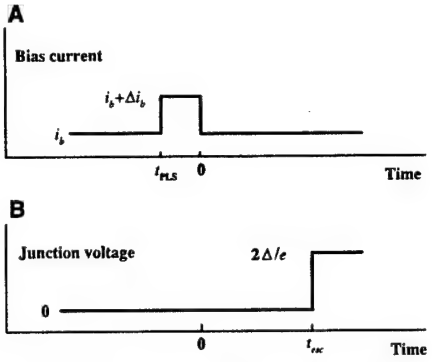

Fig. 2. (**A**) A schematic of the timing of the constant and "dc pulse" current applied to the junction. (**B**) The junction's voltage response, and the definition of t_{esc}.

In our experiment, we used a 10 μm^2 by 10 μm^2 NbN/AlN/NbN tunnel junction to measure the time-dependent escape probability at 10 mK $\leq T \leq$ 4.25 K. The junction was fabricated on a single-crystal MgO substrate at ambient temperature (*26*). The critical temperature of the junction was ~16 K. The gap energy Δ and normal state resistance R_n were 2.7 meV and 20 ohms, respectively. The critical current, I_c = 150.86 μA, was determined from switching current distribution measurements. I_c remained essentially constant below 4.2 K. The plasma frequency and capacitance of the junction, determined from resonant activation measurements (*21*), were $\omega_p/2\pi$ = 18.195 ± 0.001 GHz at 4.2 K and C = 5.8 ± 0.6 pF. C was much greater than the parasitic capacitance (<0.3 pF) of the leads within the junction's electromagnetic horizon (*27*), so the impedance loading effect of the leads was negligible. The junction was embedded in a superconducting microstrip resonator with a fundamental frequency of ~40 GHz so that it was effectively decoupled from the leads at $\omega < \omega_p$. The junction was mounted in a helium-filled oxygen-free copper cell, which was thermally anchored to the mixing chamber (MC) of a dilution refrigerator. All leads to the cell were filtered with electromagnetic interference (EMI) filters at room temperature, low-pass filters at 1.4 K, and cryogenic microwave filters (*28*) at MC temperature. A semirigid cryogenic coaxial cable, with 20 dB attenuators at 1 K plate and MC, couples microwave or dc pulses to the junction. Battery-powered low-noise preamplifiers were used to monitor the bias current and junction voltage. A solid copper shielded room, double-shielded cables, and shielded metal connectors formed a continuous conducting enclosure that extended from the sample to the battery-powered part of the setup. The computer and ac-powered instruments were placed outside the shielded room with connections via optically coupled isolation amplifiers. Measurements of the junction's voltage noise spectrum showed no peak at 60 Hz and its harmonics. Extensive diagnostic tests were performed using low critical current junctions ($I_c \sim 1$ to 10 μA) to ensure that extrinsic noise from the measurement circuit was negligible down to 10 mK.

The conventional method of measuring escape probability P_{esc} versus bias current cannot provide information about the time dependence of P_{esc} at constant i_b, so we have developed a time-domain technique with nanosecond resolution for $P_{esc}(t)$ measurement. For each escape event, we started the cycle by ramping up the bias current to a constant value i_b where escape rate was negligibly small. The bias current was maintained at this level for a short time ($\sim 10^{-3}$ s) to allow the system to reach thermal equilibrium. Using a pulse generator, a "dc pulse" of amplitude Δi_b and width $t_{PLS} \leq 1$ μs was then applied to the junction at $t = -t_{PLS}$ (Fig. 2). The pulse produced a nonequilibrium popula-

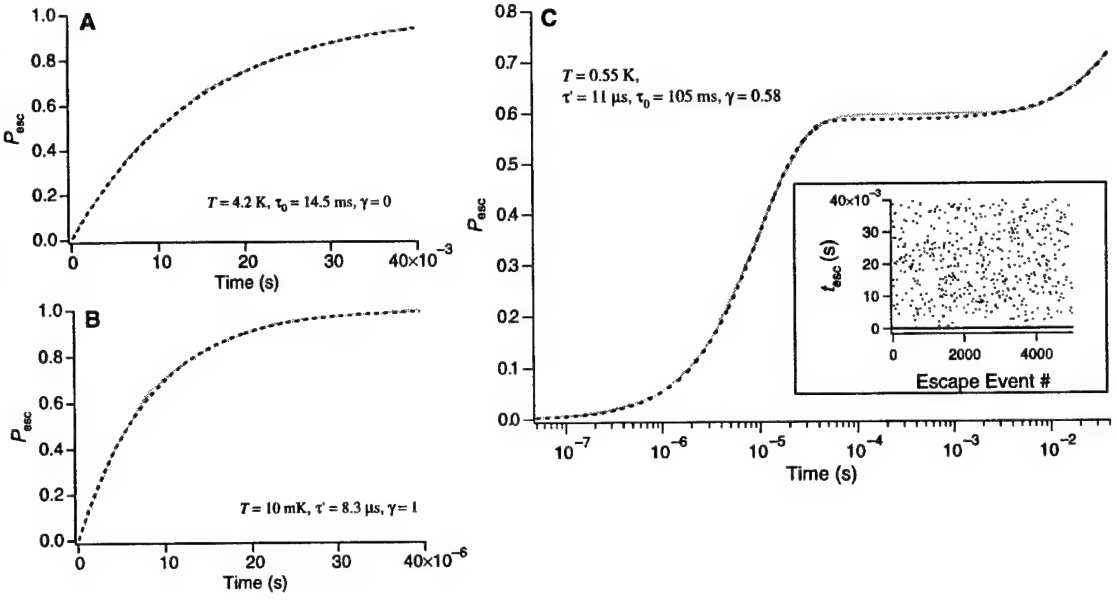

Fig. 3. Data (solid lines) of escape probability taken at **(A)** T = 4.25 K, **(B)** 0.01 K, and **(C)** 0.55 K. The dashed lines are the best fit to exponential behavior with a single (two) rate constant(s). The escape time of each event, at T = 0.55 K, is shown in the inset of (C). Bias current for (B) was slightly larger than for (C), resulting in a faster tunneling rate.

tion $\rho_{11}(0)$ through a mechanism similar to Majorana oscillation (*29*). The $\rho_{11}(0)$ can be estimated by considering the time evolution of a two-level system under a constant perturbation for a time period t_{PLS}. The Liouville equation of the time evolution of the density matrix operator, including the effects of decay and tunneling rates (Γ_d, Γ_0, and Γ_1), can be analytically solved by using the Laplace transformation, from which the time-dependent population of both levels can be obtained. The analytical expression, which is rather complicated, will be described in detail elsewhere. In the limit of Γ_d, $\Gamma_1 \ll t_{PLS}^{-1}$ a simple analytical solution can be obtained

$$\rho_{11}(0) = \frac{\chi^2}{\chi^2 + \omega^2} \sin^2\left(\sqrt{\chi^2 + \omega^2}\,\frac{t_{PLS}}{2}\right) \quad (3)$$

Here, $\hbar\omega = E_1 - E_0$ is the level spacing, $\chi = 2V_{01}/\hbar$ and V_{01} is the coupling between the two levels by the "dc pulse." The formula shows that the maximum excitation probability to the upper level is always less than unity but can be quite substantial.

The junction voltage was fed to a timer that was triggered by the sudden voltage jump when the junction switched from the zero-voltage to the finite-voltage state, to record t_{esc} (Fig. 2). i_b was then decreased to zero, resetting the junction to the zero-voltage state. The process was repeated $\sim 10^4$ times to obtain $P_{esc}(t)$.

Data were taken at T = 4.2, 0.01, and 0.55 K (Fig. 3). As expected, at the high- and low-temperature limits, the measured $P_{esc}(t)$ exhibits single-exponential behavior. In contrast, the data at T = 0.55 K display the double-exponential behavior characteristic of a TLDT process (Fig. 3C). We emphasize that this double-exponential behavior was reproducible as long as the junction was well shielded from extrinsic noises. The values of γ, $\tau_0 \equiv 1/\Gamma_0$, and $\tau' \equiv 1/\Gamma'$ obtained from the best fit are 0.58, 0.105 s, and 0.011 ms, respectively. Therefore, $\tau_d > 11$ μs, corresponding to a minimum "effective damping resistance" $R \simeq 2$ megohms according to Eq. 2. Note that the quasi-particle subgap resistance of an ideal NbN tunnel junction $R_{qp} \sim R_n e^{\Delta/k_BT} \sim 10^{25}$ ohms $\gg R$, indicating nonideal nature of the junction and the presence of other sources of dissipation (*4*). Notice that it is difficult to use this method to determine τ_d at low temperatures where $\Gamma_d \ll \Gamma_1$ unless $\rho_{11}(0)$ can be independently determined. Therefore, although it is expected that R could be greater than 2 megohms at $T \ll 0.5$ K it cannot be quantitatively verified. The data in Fig. 3, B and C, also demonstrate the nanosecond resolution of our time-domain measurement technique that opens the door to the study of temporal evolution of Josephson junctions and SQUID qubits.

In addition to τ_d, τ_φ also depends on R. For typical rf SQUID qubits

$$\tau_\varphi \simeq (\pi\alpha k_B T)^{-1} \simeq 1.5\frac{R/1\,\text{megohms}}{T/1\,mK} \quad (4)$$

where α is the quantum damping parameter (*18*) and τ_φ is in μs. For rf SQUIDs of 1 μm^2 junctions having specific resistance, R_s = 0.2 gigohms · μm^2, the most conservative estimate gives $\tau_\varphi \approx 30$ μs at 10 mK, a figure very promising for QC (*12*).

References and Notes

1. D. Loss, D. P. DiVincenzo, *Phys. Rev. A* **57**, 120 (1998).
2. B. Kane, *Nature* **393**, 133 (1998).
3. M. F. Bocko, A. M. Herr, M. J. Feldman, *IEEE Trans. Appl. Supercon.* **7**, 3638 (1997).
4. T. P. Orlando *et al.*, *Phys. Rev. B* **60**, 15398 (1999).
5. J. R. Friedman, V. Patel, W. Chen, S. K. Tolpygo, J. E. Lukens, *Nature* **406**, 43 (2000).
6. C. H. van der Wal *et al.*, *Science* **290**, 773 (2000).
7. A. Shnirman, G. Schijn, Z. Hermon, *Phys. Rev. Lett.* **79**, 2371 (1997).
8. D. V. Averin, *Solid State Commun.* **105**, 659 (1998).
9. Y. Nakamura, Y. A. Pashkin, J. S. Tsai, *Nature* **398**, 786 (1999).
10. D. J. Flees, S. Han, J. E. Lukens, *J. Supercon.* **12**, 813 (1999).
11. G. M. Palma, K. A. Suominen, A. K. Ekert, *Proc. R. Soc. London A* **452**, 567 (1996).
12. M. A. Nielsen, I. L. Chuang, in *Quantum Computation and Quantum Information* (Cambridge Univ. Press, Cambridge, ed. 1, 2000), chap. 7.
13. M. B. Plenio, P. L. Knight, *Proc. R. Soc. London A* **453**, 2017 (1997).
14. W. H. Zurek, *Phys. Today* **44** (no. 10), 36 (1991).
15. D. Braun, F. Haake, W. T. Strunz, *Phys. Rev. Lett.* **86**, 2913 (2001).
16. M. B. Plenio, P. L. Knight, *Phys. Rev. A* **53**, 2986 (1996).
17. A. I. Larkin, Y. N. Ovchinnikov, *Sov. Phys. JETP* **64**, 185 (1986).
18. A. J. Leggett *et al.*, *Rev. Mod. Phys.* **59**, 1 (1987).
19. C. Cosmelli *et al.*, *Phys. Rev. Lett.* **82**, 5357 (1999).
20. S. Han, R. Rouse, *Phys. Rev. Lett.* **86**, 4191 (2001).
21. J. Clarke, A. N. Cleland, M. H. Devoret, D. Esteve, J. M. Martinis, *Science* **239**, 992 (1988).
22. J. M. Martinis, M. H. Devoret, J. Clarke, *Phys. Rev. Lett.* **55**, 1543 (1985).
23. J. M. Schmidt, A. N. Cleland, J. Clarke, *Phys. Rev. B* **43**, 229 (1991).
24. W. Bialek, S. Chakravarty, S. Kivelson, *Phys. Rev. B* **35**, 120 (1987).
25. P. Silvestrini, V. Palmieri, B. Ruggiero, M. Russo, *Phys. Rev. Lett.* **79**, 3046 (1997).
26. Z. Wang, H. Terai, A. Kawakami, Y. Uzawa, *Appl. Phys. Lett.* **75**, 701 (1999).
27. J. P. Kauppinen, J. P. Pekola, *Phys. Rev. Lett.* **77**, 3889 (1996).
28. A. B. Zorin, *Rev. Sci. Instrum.* **66**, 4296 (1995).
29. B. W. Shore, *Simple Atoms and Fields*, vol. 1 of *The Theory of Coherent Atomic Excitation* (Wiley, New York, 1990).

30. S.H. is grateful to J. Lukens, D. Averin, and J. Martinis for stimulating comments and suggestions. The authors also acknowledge Y. Zhang, V. Patel, W. Qiu, L. Olafsen, and S. Li for technical assistance. This work was supported in part by the U.S. Air Force Office of Scientific Research (F49620-99-1-0205), the State of Kansas (S99041), and NSF (DMR9876874 and EIA0082499).

4 May 2001; accepted 24 July 2001

Appendix D

Quantitative Study of Macroscopic Quantum Tunneling in a dc SQUID: A System with Two Degrees of Freedom

Shao-Xiong Li, Yang Yu, Yu Zhang, Wei Qiu, and Siyuan Han
Department of Physics and Astronomy, University of Kansas, Lawrence, Kansas 66045

Zhen Wang
KARC, Communication Research Laboratory, Ministry of Posts and Telecommunications, 588-2 Iwaoka, Owaoka-cho, Nishi-ku, Kobe 651-24, Japan
(Received 2 October 2001; published 7 August 2002)

To test whether the theory of macroscopic quantum tunneling (MQT) is applicable to systems with 2 degrees of freedom, we experimentally investigated the switching current distribution of a dc SQUID. Using sample parameters determined from measurements at $T = 4.2$ K, we are able to make quantitative comparison to the theories from 8 mK to 4.2 K. The excellent agreement between the data and the MQT theory demonstrates that tunneling from the zero-voltage state of the dc SQUID is well described by the quantum mechanics.

DOI: 10.1103/PhysRevLett.89.098301 PACS numbers: 85.25.Dq, 03.65.–w, 74.50.+r

Whether quantum mechanics is valid for macroscopic variables is one of the most fascinating issues of fundamental physics [1]. The experimental studies, especially quantitative tests of the theory for macroscopic variables in the quantum regime, provide important insights to our understanding of the physical world. In the past few years, devices based on the Josephson effect, such as the Josephson junction (JJ) and the superconducting quantum interference device (SQUID), have been proven effective systems to perform this test. For instance, in a JJ, the phase difference δ across the junction is a macroscopic variable and the dynamics of the junction is identical to a particle's motion in a one-dimensional (1D) washboard potential. Experiments in 1D systems, such as current biased JJs and rf SQUIDs, have yielded results in very good agreement with the theoretical predictions of macroscopic quantum tunneling (MQT) [2–6]. In contrast, experiments in systems with 2 degrees of freedom (2DF) have produced significant divergences. For example, using a dc SQUID, which contains two JJs and, hence, has two macroscopic degrees of freedom, Sharifi, Gavilano, and Harlingen (SGH) reported the observation of anomalous suppression of thermal activation (TA) from the two-dimensional (2D) potential well of a dc SQUID [7]. SGH suggested that the apparent suppression of TA rate may rise from an enhanced potential barrier caused by interaction between the two macroscopic degrees of freedom in the dc SQUID. On the other hand, experiments by Han, Lapointe, and Lukens (HLL) [8] and Lefevre-Seguin, Turlot, Urbina, Esteve, and Devoret (LTUED) [9] showed that, in the thermal regime, the activation energy of the 2D SQUIDs agreed very well with the potential barrier. More importantly, SGH's result in the quantum regime significantly disagreed with the theoretical prediction as the measured width of switching current distribution-at temperature well below the quantum-classical crossover temperature T_{co}-exceeded the theoretical prediction by more than 40%. Notice that this disagreement could not be accounted for by measurement uncertainties and the barrier enhancement suggested by SGH would actually make the matter much worse. However, the HLL and LTUED's experiments did not address the quantum regime so that the experimental evidence available thus far [7] seems to indicate that, despite its great success in describing 1D systems, MQT theory might not be applicable to even the simplest 2D systems, such as dc SQUIDs with no flux bias. Furthermore, the understanding of MQT in dc SQUIDs is crucial to quantum computing with SQUID qubits, in which dc SQUIDs, as the most sensitive flux detectors available [10], serve as the readout devices. In this Letter, we report the results of a quantitative study of the escape rate of an underdamped dc SQUID, a system with 2DF, in both the TA and quantum tunneling regimes. In contrast to SGH's result, our data are in excellent agreement with the MQT theory, demonstrating that quantum mechanics also applies well to macroscopic systems with 2DF.

A dc SQUID consists of two JJs connected in parallel by a small superconducting loop of inductance L (Fig. 1 inset). The critical current of each junction is I_0 (assuming identical JJs). The macroscopic variables of this system are phases, δ_1 and δ_2, across the two junctions, respectively. For a dc SQUID with current bias I and flux bias $\Phi_e \equiv f\Phi_0$, where Φ_0 is the magnetic flux quantum, the dynamics of the system can be treated as a fictitious particle of mass C, which is the sum of the two junctions' capacitance, moving in a 2D potential [11] $U(\varphi, \varphi_{dc}) = E_J[-\cos(\varphi_{dc}/2)\cos\varphi - x\varphi + \beta_T j^2/4]$, where $E_J = \hbar I_0/e$ is the sum of two junctions' Josephson coupling energy, $\varphi \equiv (\delta_1 + \delta_2)/2$ is the average phase difference across the device, $\varphi_{dc} \equiv \delta_2 - \delta_1$, $j = (\varphi_{dc} - 2\pi f)/\beta_T$ is the normalized circulating current, $x \equiv I/2I_0$, and $\beta_T \equiv 2\pi L I_0/\Phi_0$. Figure 1 shows a 3D plot of the dc SQUID potential with zero flux bias ($f = 0$) and a small β_T value ($\beta_T = 0.3$). As one can see, in the φ (longitudinal)

 0031-9007/02/89(9)/098301(4)$20.00

direction, the potential has a sequence of saddle points and local minima (wells) located at $\varphi_{dc} = 0$, while along the φ_{dc} (transverse) direction, the potential rises sharply as $|\varphi_{dc}|$ increases. Hence, a particle initially trapped in a potential well would escape along the longitudinal direction near the vicinity of $\varphi_{dc} = 0$.

At high temperatures ($T \gg T_{co}$), escape from the 2D potential well is dominated by TA over the potential barrier with the transition rate given by [11,12]

$$\Gamma = \frac{\Omega}{2\pi} a_t \exp\left(-\frac{\Delta U}{k_B T}\right), \tag{1}$$

where ΔU is the minimum height of the potential barrier (i.e., through the saddle point), T is temperature, and a_t ($0 < a_t < 1$) is a damping dependent factor [13]. The "attempt frequency" Ω is given by $\Omega \equiv \omega_{lw}(\omega_{tw}/\omega_{ts})$, where $\omega_{lw}(\omega_{tw})$ is longitudinal (transverse) small oscillation frequency in the well, and ω_{ts} is the transverse oscillation frequency at the saddle. Equation (1) is equivalent to the TA rate of a 1D system having the attempt frequency renormalized by a factor of ω_{tw}/ω_{ts}. For dc SQUIDs with $\beta_T \ll 2\pi$, such as the one studied here and in [7], the ratio ω_{tw}/ω_{ts} is close to unity. Hence, the TA rate of dc SQUIDs with $\beta_T \ll 2\pi$ should closely follow that of a 1D system.

At $T \ll T_{co}$, MQT becomes the dominant escape mechanism. The tunneling rate of dc SQUIDs with $f = 0$ is given by [14]:

$$\Gamma = f_{2D}(\alpha, \alpha_c)\frac{\omega_0}{2\pi}\sqrt{120\pi}\left(7.2\frac{\Delta U}{\hbar\omega_0}\right)^{1/2}\exp\left(-7.2\frac{\Delta U}{\hbar\omega_0}\right)$$
$$= f_{2D}(\alpha, \alpha_c)\Gamma_{1D}, \tag{2}$$

where $\omega_0 = (2\pi I_0/C_J\Phi_0)^{1/2}(1 - x^2)^{1/4}$ is the plasma frequency and C_J is the shunt capacitance of each junction. $f_{2D}(\alpha, \alpha_c)$ is a dimensionless function of $\alpha \equiv 2\sqrt{2}\beta_T^{-1} \times (1 - x)^{-1/2}$ and $\alpha_c \equiv -90\exp(-2\pi T_{co}/T) + 5/4$, where α is a measure of interaction between the 2DF, α_c is the critical parameter for instanton splitting, and $T_{co} = \hbar\omega_0/2\pi k_B$ is the quantum-thermal crossover temperature. Equation (2) clearly shows that the tunneling rate of a dc SQUID with zero flux is closely related to that of a single Josephson junction. In particular, for dc SQUIDs with $\beta_T \ll 2\pi$, such as our sample and that of SGH ($\beta_T \simeq 0.4$), there is no instanton splitting and $f_{2D} \simeq 1$. Notice that the disagreement between the result of [7] and the MQT theory is so significant that no reasonable adjustment of sample parameters could reconcile the data with Eq. (2).

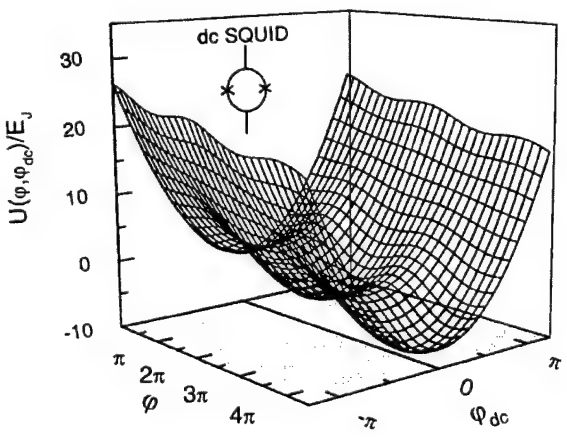

FIG. 1. The 2D potential for a dc SQUID with $f = 0$, $\beta_T = 0.3$, and $x \equiv I_b/2I_0 = 0.25$. The inset is a schematic of the dc SQUID.

The switching current distribution $P(x)$ is related to the escape rate through

$$P(x) = \frac{\Gamma(x)}{dx/dt}\exp\left[-\frac{1}{dx/dt}\int_0^x \Gamma(x')dx'\right]. \tag{3}$$

To quantitatively compare experimental data with various theories, it is convenient to use the "escape temperature" T_{esc} defined through [15] $\Gamma = \Omega/2\pi\exp(-\Delta U/k_B T_{esc})$. It is straightforward to show that, for TA $T_{esc} \simeq T$, while for quantum tunneling $T_{esc} \simeq T_{co}$. For dc SQUIDs biased at $x \lesssim 1$, T_{esc} depends linearly on $\sigma^{3/2}$ [16], where σ is known as the width of $P(x)$. Because in our experiment the widths were extracted directly from the measured $P(x)$, which did not involve the use of any theoretical model and sample parameter, it was used in our data analysis and presentations.

The sample was a dc SQUID consisting of two nominally identical NbN/AlN/NbN JJs each having a diameter of 2 μm. The critical current of the dc SQUID is $2I_0 = 35.8$ μA, which was determined by fitting $P(x)$ at 4.2 K, where the system was in the thermal regime. Because of the large energy gap of NbN ($2\Delta \simeq 5.4$ meV), I_0 remained constant below 4.2 K. Notice that in the quantum regime it is essential to have an independent measurement of the sample's shunt capacitance for making a quantitative comparison between the data and theoretical predictions. In our experiment, the capacitance of the dc SQUID, $C = 2C_J = 380 \pm 30$ fF, was determined from resonant activation (RA) measurement [15] at 4.2 K. The RA data also yielded a quality factor, $Q \equiv RC\omega_0 \approx 200$, indicating that the effect of damping on tunneling at $T \ll T_{co}$ was negligible [17,18]. The inductance of the dc SQUID loop, estimated from the modulation depth of critical current and loop geometry, is $L = 5 \pm 1$ pH. Using these sample parameters, the crossover temperature is found to be $T_{co} = 0.29$ K.

We measured the switching current distribution of the dc SQUID using a time-of-flight technique similar to that described in [19]. Each measured distribution consisted of $2 \times 10^4 20\,000$ escape events. Because heating and external noise could cause the width σ to flatten out at low temperatures, which could be mistaken as the evidence for MQT, cautions must be taken to eliminate them. In our experiment, the dc SQUID was enclosed in a helium-filled copper sample cell thermally anchored to the mixing chamber of a dilution refrigerator. EMI filters, cryogenic low-pass filters and microcoax microwave filters [20],

battery-powered low-noise preamplifiers, and shielded enclosure were used to protect the sample from external noise. Connections to the computer and ac-powered instruments were made via optically coupled isolation amplifiers. Extensive diagnostic tests were made using low critical current ($I_c \sim 1$–$10\ \mu$A) junctions to ensure that the effects of noise from the environment and measurement circuitry was negligible down to 8 mK. Distributions with $\sigma < 15$ nA have been observed using the same setup, demonstrating the effectiveness of the shielding. A mu-metal cylinder provided ~60 dB attenuation to shield the sample from ambient magnetic field fluctuations. For improved stability, the data were taken with zero flux bias ($f = 0$) and the temperature was regulated to within $\pm 1\%$ and $\pm 0.3\%$ of the set point at T below and above 0.6 K, respectively.

Figure 2 shows a series of measured switching current distributions and their comparisons with the 2D TA and MQT theories. Notice that Eq. (3) is valid if the temporal escape probability at constant bias currents was $P_{esc}(t) = 1 - e^{-\Gamma t}$, which was confirmed by the measured $P_{esc}(t)$ shown in Fig. 2(a). The data in Fig. 2 show that, in both the thermal ($T > 2T_{co}$) and quantum ($T > T_{co}/2$) regimes, the distributions, including their shape, width, and position, agree very well with the theoretical predictions. Below 0.15 K the data were essentially the same, as expected for a system with very low damping [17,18]. Tunneling rates obtained from the switching current distributions are plotted as a function of barrier height in Fig. 3. Considering that all theoretical calculations were performed using the sample parameters determined from measurements at 4.2 K, the agreement between the data and theories is quite remarkable. Our data provide strong evidence supporting the validity of MQT theory for systems with 2DF.

However, as shown in Fig. 2(b), in the crossover region the measured distributions deviate significantly from that of $T = 0$ MQT theory (the dashed line). By taking into account the effects of thermal enhancement to MQT [17], the agreement between the data and theory (the solid line) improves. However, the remaining disagreement cannot be entirely accounted by the thermally enhanced MQT theory, indicating the need for further studies in this temperature range, where neither TA nor MQT is the dominant escape mechanism.

A critical comparison of the experimental data and various theories can be obtained by examining the T dependence of the distribution width [21]. In Fig. 4 and its inset, the measured σ vs $T^{2/3}$ is compared with the MQT and TA theories using the sample parameters $2I_0 = 35.8\ \mu$A, $C = 380$ fF, and $R = 1500\ \Omega$. At $T > 0.6$ K, the data show a linear dependence on $T^{2/3}$, as expected from Eq. (1) of TA theory (the solid line) without adjustable parameters. The excellent quantitative agreement between the data and the theory of TA clearly shows that the activation energies were equal to the 2D potential barriers, in agreement with the results of HLL and LTUED. Below $T = 0.15$ K, the data became T independent within the uncertainties of measurements. In the quantum limit, the measured $\sigma_{data}(T \leq 0.15\ \text{K}) = 40.6 \pm 1.6$ nA is consistent with the 41.2 nA calculated from the $T = 0$ MQT theory (the dashed line). Notice that in the thermal

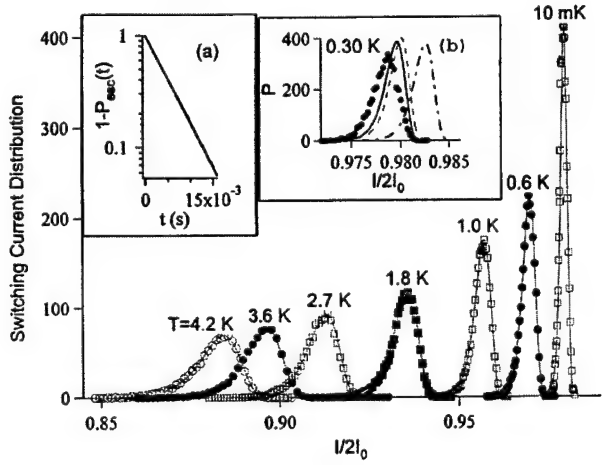

FIG. 2. The measured temperature dependence of the switching current distributions. The symbols are the experimental data and the lines are calculated from the theories of thermal activation and MQT for systems with 2DF. Inset (a): The temporal escape probability at bias $x = 0.975$ and $T = 10$ mK showing the expected exponential decay. Inset (b): Comparison of the measured distribution (solid dots) at $T = 300$ mK with the theoretical prediction of quantum correction (solid line), $T = 0$ MQT (dashed line), and thermal activation (dash-dotted line).

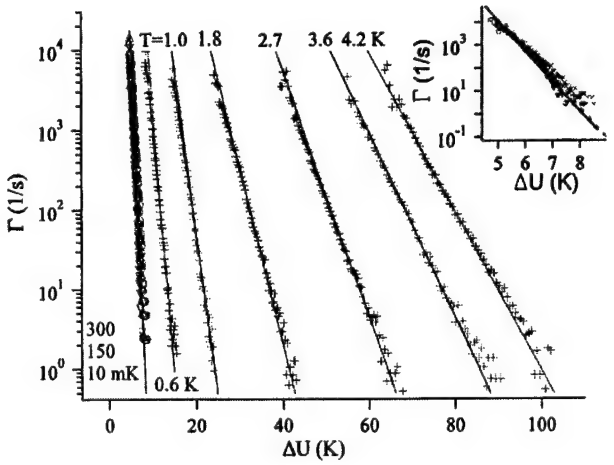

FIG. 3. Tunneling rates vs potential barrier at various temperatures. The symbols are data and the solid lines are theoretical predictions. The first three data sets from the left are $T = 10$ mK (triangles), 150 mK (circles), and 300 mK (crosses). Inset: The measured (symbols) and predicted (lines) tunneling rates vs barrier height for $T = 10$ mK (triangles and solid line), 150 mK (circles and dotted line), and 300 mK (crosses and dashed line).

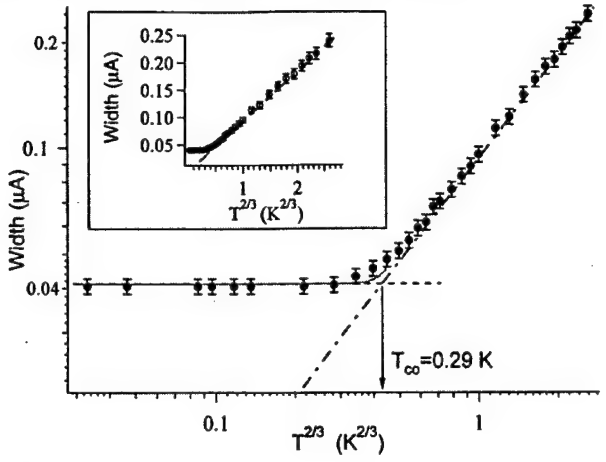

FIG. 4. σ vs $T^{2/3}$ of the data (symbols) and the predictions of thermally enhanced quantum tunneling of Ref. [12] (solid line), thermal activation (dot-dashed line), and 2D MQT (dashed line) with arrow indicating T_{co}. The log-log plot magnifies the low temperature region, while the inset shows the linear dependence of σ on $T^{2/3}$ in the thermal regime.

limit, for samples with $Q \gg 1$, σ is almost independent of C but quite sensitive to R. The situation is just the opposite in the quantum regime. For instance, using $C = 395$ fF, we found $\sigma = 40.6$ nA$=\sigma_{data}(T \leq 0.15$ K), while increasing R from 1.5 kΩ to 1.5 MΩ results in a negligible change in the calculated width. Hence, the data at $T < 0.15$ K again show that in the quantum regime the MQT theory describes the behavior of a system of 2DF very well.

Finally, we examine the crossover region. From the interception of the straight lines extrapolated from the data in quantum and thermal limits, we found $T_{co} = 0.29 \pm 0.01$ K, which agrees very well with the theoretical value of 0.290 K calculated from the sample parameters. However, for $0.15\ \text{K} < T < 0.6$ K, the measured $\sigma_{data}(T)$ deviates systematically from both the T-independent behavior of the MQT theory and the simple $\sigma \propto T^{2/3}$ scaling behavior of the TA theory (Fig. 4). Similar smooth crossover behavior was observed previously in Josephson junctions by Martinis *et al.* [5]. Because in both the thermal and quantum limits the data agree very well with the theoretical predictions, the larger width in the crossover region could not be due to heating or external noise. One mechanism that could result in a larger width is the thermal enhancement of MQT, which produces an improved, albeit still unsatisfactory, agreement with the data for $0.15\ \text{K} < T < T_{co}$. For $T_{co} < T < 0.6$ K, the theory of quantum correction [17] produced negligible improvement. In the crossover region, the shape of $P(x)$ also significantly deviates from that calculated from Eq. (3), which could occur when tunneling from excited levels contributes significantly to the escape process [19].

In summary, we have measured the temperature dependence of the switching current distributions of a dc SQUID from well below ($< 0.025T_{co}$) to well above ($\sim 14T_{co}$) the quantum-classical crossover temperature. The experimental ability to control and characterize the sample and the theoretical capability to accurately model the system facilitate a quantitative comparison between the theories and experiment. Our result in the thermal regime agrees very well with the works of HLL and LTUED, supporting the TA theory. More importantly, without the use of adjustable parameters, the data in the quantum regime agree excellently with the MQT theory, demonstrating incontrovertibly that the theory of MQT correctly describes the behavior of dc SQUIDs—a macroscopic quantum system with 2DF. The result also assures that the MQT theory can be applied to design the readout circuits made of dc SQUIDs for flux based superconducting quantum logic gates.

We thank R. Alexander for technical support. This work was supported in part by AFOSR (F49620-99-1-0205), the state of Kansas (S99041), and the NSF (DMR-9876874).

[1] *Quantum Tunneling in Condensed Media*, Modern Problems in Condensed Matter Sciences Vol. 34, edited by Y. Kagan and A. J. Leggett (North-Holland, Amsterdam, 1992).
[2] R. F. Voss and R. A. Webb, Phys. Rev. Lett. **47**, 265 (1981).
[3] S. Washburn, R. A. Webb, R. F. Voss, and S. M. Faris, Phys. Rev. Lett. **54**, 2712 (1985).
[4] D. B. Schwartz, B. Sen, C. N. Archie, and J. E. Lukens, Phys. Rev. Lett. **55**, 1547 (1985).
[5] M. H. Devoret, J. M. Martinis, and J. Clarke, Phys. Rev. Lett. **55**, 1908 (1985).
[6] J. Clarke *et al.*, Science **239**, 992 (1988).
[7] F. Sharifi, J. L. Gavilano, and D. J. V. Harlingen, Phys. Rev. Lett. **61**, 742 (1988).
[8] S. Han, J. Lapointe, and J. Lukens, Phys. Rev. Lett. **63**, 1712 (1989).
[9] V. Lefevre-Seguin *et al.*, Phys. Rev. B **46**, 5507 (1992).
[10] M. Mück, J. B. Kycia, and J. Clarke, Appl. Phys. Lett. **78**, 967 (2001).
[11] C. D. Tesche, J. Low Temp. Phys. **44**, 119 (1981).
[12] E. Ben-Jacob *et al.*, J. Appl. Phys. **54**, 6533 (1983).
[13] M Büttiker, E. P. Harris, and R. Landauer, Phys. Rev. B **28**, 1268 (1983).
[14] B. I. Ivlev and Y. N. Ovchinnikov, Sov. Phys. JETP **66**, 378 (1987).
[15] J. M. Martinis, M. H. Devoret, and J. Clarke, Phys. Rev. B **35**, 4682 (1987).
[16] J. Kurkijärvi, Phys. Rev. B **6**, 832 (1972).
[17] H. Grabert, P. Olschowski, and U. Weiss, Phys. Rev. B **36**, 1931 (1987).
[18] A. O. Caldeira and A. J. Leggett, Ann. Phys. (N.Y.) **149**, 374 (1983).
[19] S. Han *et al.*, Science **293**, 1457 (2001).
[20] A. B. Zorin, Rev. Sci. Instrum. **66**, 4296 (1995).
[21] A. Garg, Phys. Rev. B **51**, 15 592 (1995).

Appendix E

Efficiency of Underdamped dc SQUIDs as Single-Shot Readout Devices of Flux Qubit

Shaoxiong Li, Yang Yu, Wei Qiu, Siyuan Han and Zhen Wang

Abstract—**Flux state quantum bit (qubit) is promising for solid state implementation of scalable quantum computing. The simplest flux state qubit consists of an rf SQUID with two fluxoid states, which can be readout with a dc SQUID – the most sensitive magnetic flux detector. In order to minimize the influence (back-action, noise, etc.) of the readout dc SQUID on the qubit, one must decouple the detector sufficiently from the qubit. On the other hand, stronger coupling between the detector and the qubit is advantageous for reliable single-shot readout. In this work, we report the measurements of the switching flux and switching current distributions of underdamped dc SQUIDs and their implications on the design of rf SQUID qubit with dc SQUID readout circuit**

Index Terms—**Qubit, Readout, dc SQUID.**

Quantum computing has drawn significant interests because of its massive intrinsic parallelism. In principle, any system that is able to store and coherently process information in a Hilbert space can be used to implement quantum computing. Recently, quantum logic operations have been demonstrated in several physical systems such as trapped ions [1], NMR [2], quantum electrodynamics cavities [3], and Josephson devices [4]. Because, distinguished from the other candidates for constructing qubit, the solid state Josephson device is scalable and its parameters are readily adjustable, Josephson qubits are recognized as a very promising approach to quantum computing. Based on the two quantum conjugate variables - charge and phase (flux)- Josephson qubits can be divided into two main types: the charge qubit and the flux qubit. Comparing with the charge qubit, the flux qubit has the advantage of being insensitive to background charge fluctuation which is a major source of decoherence. From a practical point of view, a strong single-shot readout measurement of qubit is needed for not only getting the final result of the quantum computation but also the purpose of error correction in the course of the computation. However, a strong readout measurement usually results in a significant back-action on the qubit, which in turn causes gate errors and dephasing. Therefore, a detailed study on the sensitivity and efficiency of dc SQUIDs as the readout devices of the flux qubits is instructive. In this work, the magnetic modulation of switching current, the switching flux and switching current distributions, and the efficiency of underdamped dc SQUIDs as qubit state readout devices are presented and discussed.

The best device to measure the fluxoid state of an rf SQUID-flux qubit is probably the dc SQUID, which is well known as the most sensitive magnetometer. A dc SQUID consists of a superconducting loop of inductance L_{dc}, interrupted by two Josephson junctions with a total critical current I_c. Because of the bi-directional inductive coupling to the qubit, underdamped dc SQUIDs, which introduce much weaker dissipation and noise to the qubit, is more desirable

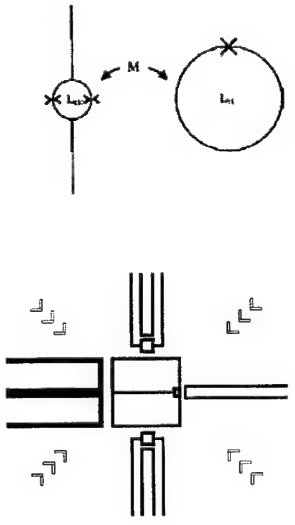

Fig. 1. Top: the equivalent circuit of a flux qubit coupled to a dc SQUID readout device through mutual inductance *M*. Bottom: the layout of a sample which has a gradiometer flux qubit inductively coupled to unshunted dc SQUID detectors.

Manuscript received August 6, 2002. This work was supported by AFOSR (F49620-99-1-0205), AFOSR and ARDA (F49620-01-1-0439), the State of Kansas (S99041), and NSF (DMR9876874).

Shaoxiong Li, Yang Yu, Wei Qiu, and Siyuan Han are with the Department of Physics and Astronomy, University of Kansas, Lawrence, KS 66044, USA (corresponding author to provide phone: 785-864-5831; fax: 785-864-5265; e-mail: han@ku.edu).

Zhen Wang is with Kansai Advanced Research Center, Communication esearch laboratory, Ministry of Posts and Telecommunications, 588-2 Iwaoka, Iwaoka-cho, Nishi-ku, Kobe, 651-24 Japan.

than the conventional overdamped dc SQUID magnetometers.

A simple dc SQUID measurement setup for a flux qubit (rf SQUID) is shown in Fig. 1. In the following, we will focus our discussions on two readout methods: the sweeping-current and the sweeping-flux detection modes. For the sweeping-current mode, one ramps the bias current of the dc SQUID up while keeping the flux bias constant until it switches to the finite voltage state. From the value of the switching current I_S, one can get the information about the flux state of the qubit because the switching current is sensitive to the amount of externally applied flux $\Phi_{xdc} = \Phi_{xs} + MI_{cir}(f)$ in the dc SQUID loop. Here, Φ_{xs} is the quasi-static flux bias of the detector, M the mutual inductance between the qubit and the detector, and $I_{cir}(f)$ is the circulation current of the qubit which depends on the fluxoid state ($f = 0, 1$) of the qubit. Because the dc SQUID's critical current, thus the switching current, is a function of Φ_{xdc}, the state of qubit can be inferred by measuring the switching current I_s of the detector. For instance, for $\Phi_{xs}/\Phi_0 \approx 0.25$ switching current is higher when the qubit is in the $|0\rangle$ ($f = 0$) state, *i.e.*, $I_s(f=0) > I_s(f=1)$ because of the negative slope of $I_s(\Phi_{xdc})$ function, assuming the qubit-detector is weakly coupled ($M|I_{cir}|/\Phi_0 \ll 1$). Similarly, for the sweeping-flux mode of readout, one ramps up the flux bias of the dc SQUID, while keeping the bias current constant, until the detector switches to the $V \neq 0$ state. The value of the flux bias at which the detector switches depends on whether the qubit is in the $|0\rangle$ or the $|1\rangle$ state. Furthermore, these readout procedures can be improved by implementing simple changes. For example, to reduce back-action when operated in the sweeping-current readout mode one can set the maximum bias current to a level that is about halfway between $I_s(f=1)$ and $I_s(f=0)$ so that the detector will switch only if the qubit was in the $|1\rangle$ state.

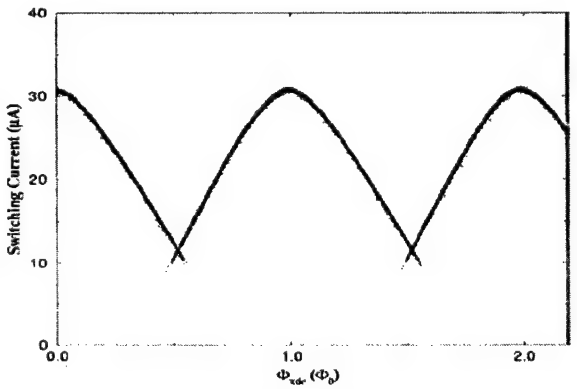

Fig. 2. The flux modulation of the switching current of the dc SQUID at T=1.55 K.

The circuit studied here was a variable barrier rf SQUID flux qubit inductively coupled to an unshunted dc SQUID detector. The qubit has a $L_{rf} \approx 200$ pH superconducting loop that is interrupted by two NbN/AlN/NbN Josephson tunnel junctions in parallel by a low-inductance loop. The dc SQUID detector has two nominally identical 2×2 μm^2 NbN/AlN/NbN Josephson tunnel junctions. The total critical current of the dc SQUID is $I_c \approx 33$ μA, the capacitance is $C \approx 448$ fF, and the loop inductance is $L_{dc} \approx 30$ pH. The mutual inductance between the qubit and the dc SQUID is $M \approx 2.9$ pH, which is determined from the measured flux dependence of switching current and the size of the flux jump produced by the qubit switching from one to the other fluxoid state.

Fig. 2. shows the magnetic modulation of the dc SQUID's switching current $I_s(\Phi_{xd})$ taken at T =1.55 K. During the measurement, the qubit state was unchanged. The flux modulation of I_s is obtained by repeatedly ramping up and down the bias current of the dc SQUID while slowly (quasi-statically) increasing the magnetic flux applied to the dc SQUID loop at the same time. The typical periodic flux dependence of the switching current was observed. It is well known that switching from the zero voltage state to the finite voltage state is a random process, and that the switching currents at a constant flux obey certain statistical distribution [5]. From Fig. 2 one can see that the distribution is slightly wider for larger switching currents and narrower for small switching currents, as expected from theory. The double peak distribution in the vicinity of the minimum switching current is caused by the emergence of a second set of metastable potential wells in dc SQUIDs that have large value of $\beta_T \equiv 2\pi L_{dc} I_0 / \Phi_0$.

Fig. 3. shows the rf SQUID's hysteretic loop detected by the dc SQUID at 4.2 K. The horizontal axis is the flux applied

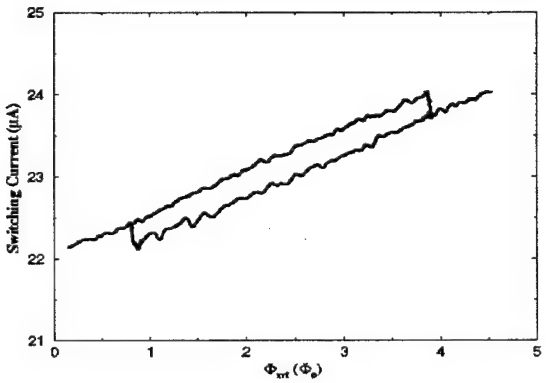

Fig. 3. The rf SQUID's hysteretic loop detected by the dc SQUID switch at 4.2 K. Higher (lower) switching currents correspond to the $|0\rangle$ ($|1\rangle$) qubit state.

to the rf SQUID and the vertical axis is the average switching current $\overline{I_S}$ of the dc SQUID detector. The sudden jumps in

$\overline{I_s}$ correspond to the qubit changing state from $|0\rangle$ to $|1\rangle$ and vice versa. Here, we define the fluxoid states of the rf SQUID qubit with a negative circulation current as the $|0\rangle$ state and the state with opposite circulating current as the $|1\rangle$ state. From Fig. 3 one can see that a transition between these two fluxoid states induces a signal of $\Delta\overline{I}_S \approx 0.3$ μA. It is obvious that the size of the switching current jump and the widths of the corresponding switching current distributions determine the single-shot detection efficiency (SSDE) of the sweeping-current readout mode. It is straightforward to show that a narrower width of the switching current distribution (SCD) and a larger ΔI_s result in a higher SSDE. However, because $\Delta I_s \simeq 2M\left[I_{cir}(1)-I_{cir}(0)\right](\partial I_s/\partial\Phi_{xd}) \propto M$ and the terms in the brackets depend only on the device parameters of the detector and qubit increasing signal means larger M and thus stronger back-action, which is undesirable. Therefore, SSDE should be improved without increasing the coupling between the detector and qubit. This can be done by reducing the width of the switching current distributions, which can be achieved by increasing the capacitance and/or decreasing the critical current of the dc SQUID detector. It has been shown recently that in both the classical (thermal) and quantum regimes the switching current distributions of dc SQUIDs agree very well with the theoretical predictions of thermal activation and macroscopic quantum tunneling (MQT) [6]. For the detector used in this experiment the minimum width of SCD is expected to be about 40 nA. Hence, the overlap between two such switching current distributions with their position separated by about 0.3 μA, is less than 0.01%, corresponding to $SSDE > 99.99\%$ at temperatures below the classical-quantum crossover temperature of 0.26 K (see Fig. 4).

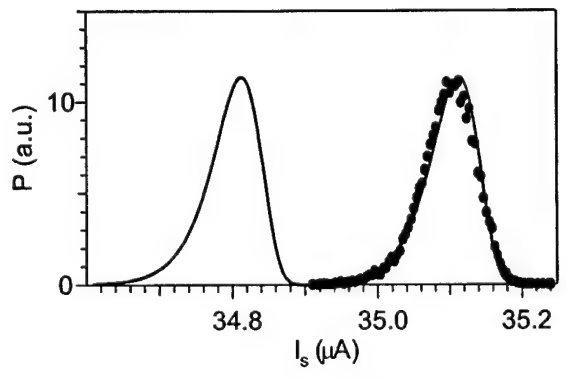

Fig. 4. The flux distributions of the two fluxoid states of the rf SQUID at T=0.26 K, results in a single-shot detection efficiency of about >99.9%.

Fig. 5. shows the two switching flux distributions of the dc SQUID at $T = 1.4$ K. The left distribution was taken when the qubit was in the $|0\rangle$ state while the right one taken with the qubit in the $|1\rangle$ state. The solid circles are data which agree with the theoretical predictions (solid lines) very well. The width of the left distribution in Fig. 5 is $\sigma_{|1\rangle} \simeq 7.2\,\mathrm{m}\Phi_0$ and the right is $\sigma_{|1\rangle} \simeq 6.9\,\mathrm{m}\Phi_0$ respectively. The horizontal distance between the peaks of the two switching flux distributions is about 14.4 $\mathrm{m}\Phi_0$. The efficiency of sweeping-flux readout mode can then be evaluated by integrating the overlapping part of the two distributions. At $T = 1.4$ K the overlap was about 1.2%, corresponding to a single-shot detection efficiency of 98.8%. Notice that similar to the sweeping-current mode, SSDE of the sweeping-flux mode can also be significantly improved by cooling the dc SQUID to temperatures well below the classical-quantum crossover temperature. Therefore, although using an unshunted dc SQUID to detect the state of a flux qubit is intrinsically a statistical measurement, our data show that for flux qubit the single-shot measurement can be realized if the parameters of the dc SQUID are properly chosen.

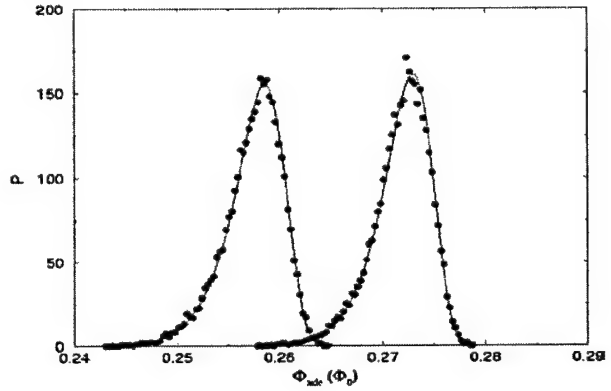

Fig. 5. The flux distributions of the two fluxoid states of the rf SQUID at T=1.4 K, gives a single-shot detection efficiency of about 98%.

As mentioned before that stronger coupling between qubit and detector leads to larger signal, and thus higher readout efficiency. Unfortunately, the increasing coupling will also result in stronger back-action that causes gate errors and decoherence in the qubit. Therefore, from the point of view of reducing back-action from the detector to the qubit one must keep the coupling as weak as possible. In the following discussions we estimate the amount of back-action generated from ramping the dc SQUID's bias current. For the qubit-detector circuit tested in this experiment the back-action flux is $MI_{dc} \approx 1.4\times10^{-2}\,\Phi_0$, where $I_{dc} \approx 10\,\mu$A is assumed the typical value of dc SQUID's bias current. Since a change of less than $1\,\mathrm{m}\Phi_0$ in flux bias is large enough to significantly alter the energy level spectrum of a typical rf SQUID flux qubit this amount of back-action cannot be tolerated and need to be reduced by about a factor of 1000. This can be achieved by the use of detectors with much smaller critical current and clever qubit-detector coupling schemes. One of the ways is to decouple the external (symmetric) mode of the dc SQUID's current from the qubit while maintaining sufficient coupling

between the internal mode (i.e., circulating current) of the detector and the qubit. Another way of having sufficient readout efficiency while keeping back-action to minimum is to use variable flux transformers so that the coupling between the qubit and detector can be switched on/off *in situ*. [7].

Finally, let's examine the amount of additional damping introduced onto a flux qubit from a dc SQUID detector. For this purpose the detector can be modeled as a resistor R_{dc} in parallel with an inductor L_{dc} which is coupled to the qubit through a mutual inductance M. It is straightforward to show that for frequency $\omega \ll R_{dc}/L_{dc}$ the effect of the detector is equivalent to shunt the qubit with an effective damping resistor $R_{eff} = (L_{rf}/M)^2 R_{dc}$. Because R_{eff} is a increasing function of frequency its effect becomes much weaker at high frequencies ($\omega \gg R_{dc}/L_{dc}$). Taking a typical value of $L_{rf}/M \approx 100$ and $R_{dc} \approx 1\,\mathrm{k\Omega}$ for unshunted dc SQUIDs, we found $R_{eff} \approx 10\,\mathrm{M\Omega}$, which will have negligible effect on the energy relaxation and dephasing of the flux qubits.

In summary, the switching current and switching flux distributions of unshunted dc SQUIDs detectors were measured at various temperatures. The results show that when used as the readout device for rf SQUID flux qubits one can achieve very high efficiency single-shot detection so that the readout can almost be regarded as deterministic. In addition,it is shown that detectors with small critical current and low crossover temperature (e.g., large capacitance) are desirable for having higher SSDE and weaker back-action. Finally, it is also shown that the amount of additional damping onto the flux qubits from the dc SQUID detectors is negligible.

REFERENCES

[1] C. Monroe, D. M. Meekhof, B. E. King, W. M. Itano, D. J. Wineland, "Demonstration of a Fundamental Quantum Logic Gate", *Phys. Rev. Lett.* **75**, pp. 4714-4717, (1995).

[2] N. A. Gershenfeld and I. L. Chang, "Bulk Spin-Resonance Quantum Computation", *Science* **275**, pp. 350, (1997).

[3] Q. A. Turchette, C. J. Hood, W. Lange, H. Mabuchi, H. J. Kimble, "Measurement of Conditional Phase Shifts for Quantum Logic", *Phys. Rev. Lett.* **75**, pp. 4710-4713, (1995).

[4] For a review, see Y. Makhlin, G. Schön, and A. Shnirman, "Quantum-state engineering with Josephson-junction devices", *Rev. Mod. Phys.* **73**, pp. 357, (2001).

[5] J. Kurkijarvi, "Intrinsic Fluctuations in a Superconducting Ring Closed with a Josephson Junction", Phys. Rev. B **6**, pp. 832 (1972).

[6] Shao-Xiong Li, Yang Yu, Yu Zhang, Wei Qiu, and Siyuan Han, "Quantitative Study of Macroscopic Quantum Tunneling in a dc SQUID: A System with Two Degrees of Freedom", *Phys. Rev. Lett.* in press, (2002).

[7] J. E. Lukens, private communication, (2002).

Appendix F

This loss of contrast is likely to be due to a relaxation of the level population during the measurement itself.

In order to understand what limits the coherence time of the circuit, measurements of the linewidth $\Delta\nu_{01}$ of the resonant peak as a function of U and Φ have been performed. The linewidth increases linearly when departing from the optimal point ($N_g = 1/2$, $\phi = 0$, $I_b = 0$). This dependence is well accounted for by charge and phase noises with root mean square deviations $\Delta N_g = 0.004$ and $\Delta(\delta/2\pi) = 0.002$ during the time needed to record the resonance. The residual linewidth at the optimal working point is well explained by the second-order contribution of these noises. The amplitude of the charge noise is in agreement with measurements of $1/f$ charge noise (*31*), and its effect could be minimized by increasing the E_J/E_{CP} ratio. The amplitude of the flux noise is unusually large (*32*) and should be significantly reduced by improved magnetic shielding. An improvement of Q_φ by an order of magnitude thus seems possible. Experiments on quantum gates based on the controlled entanglement of several capacitively coupled quantronium circuits could already be performed with the level of quantum coherence achieved in the present experiment.

References and Notes

1. M. A. Nielsen, I. L. Chuang, *Quantum Computation and Quantum Information* (Cambridge Univ. Press, Cambridge, 2000).
2. *The Physics of Quantum Information: Quantum Cryptography, Quantum Teleportation, Quantum Computation*, D. Bouwmeester, A. Ekert, A. Zeilinger, Eds. (Springer-Verlag, Berlin, 2000).
3. V. B. Braginsky, F. Ya. Khalili, *Quantum Measurement* (Cambridge Univ. Press, 1992).
4. W. H. Zurek, J. P. Paz, in *Coherent Atomic Matter Waves*, R. Kaiser, C. Westbrook, F. David, Eds. (Springer-Verlag, Heidelberg, Germany, 2000).
5. P. W. Shor, *Phys. Rev. A* **52**, R2493 (1995).
6. A. M. Steane, *Phys. Rev. Lett.* **77**, 793 (1996); *Rep. Prog. Phys.* **61**, 117 (1998).
7. J. Preskill, *J. Proc. R. Soc. London Ser.* A **454**, 385 (1998)
8. Y. Makhlin, G. Schön, A. Shnirman, *Rev. Mod. Phys.* **73**, 357 (2001).
9. M. H. Devoret *et al.*, in *Quantum Tunneling in Condensed Media*, Y. Kagan, A. J. Leggett, Eds. (Elsevier Science, Amsterdam, 1992).
10. Y. Nakamura, Yu. A. Pashkin, J. S. Tsai, *Nature* **398**, 786, (1999).
11. C. H. van der Wal *et al.*, *Science* **290**, 773 (2000).
12. S. Han, R. Rouse, J. E. Lukens, *Phys. Rev. Lett.* **84**, 1300 (2000).
13. S. Han, Y. Yu, X. Chu, S. -I. Chu, Z. Wang, *Science* **293**, 1457 (2001).
14. J. M. Martinis, S. Nan, J. Aumentado, and C. Urbina (unpublished data) have recently obtained Q_φ's reaching 1000 for a current-biased Josephson junction.
15. Y. Nakamura, Yu. A. Pashkin, T. Yamamoto, J. S. Tsai, *Phys. Rev. Lett.* **88**, 047901 (2002).
16. V. Bouchiat, D. Vion, P. Joyez, D. Esteve, M. H. Devoret, *Phys. Scr.* **T76**, 165 (1998).
17. A. Cottet *et al.*, *Physica C* **367**, 197 (2002).
18. Another two-port design has been proposed by A. B. Zorin [*Physica C* **368**, 284 (2002)].
19. M. T. Tuominen, J. M. Hergenrother, T. S. Tighe, M. Tinkham, *Phys. Rev. Lett.* **69**, 1997 (1992).
20. P. Lafarge, P. Joyez, D. Esteve, C. Urbina, M. H. Devoret, *Nature* **365**, 422 (1993).
21. D. V. Averin, K. K. Likharev, in *Mesoscopic Phenomena in Solids*, B. L. Altshuler, P. A. Lee, R. A. Webb, Eds. (Elsevier, Amsterdam, 1991).
22. J. R. Friedman, D. V. Averin, *Phys. Rev. Lett.* **88**, 50403 (2002).
23. A. Aassime, G. Johansson, G. Wendin, R. J. Schoelkopf, P. Delsing, *Phys. Rev. Lett.* **86**, 3376 (2001).
24. A different Cooper pair box readout scheme using a large Josephson junction is discussed by F. W. J. Hekking, O. Buisson, F. Balestro, and M. G. Vergniory, in *Electronic Correlations: From Meso- to Nanophysics*, T. Martin, G. Montambaux, J. Trân Thanh Vân, Eds. (Editions De Physique, Les Ulis, France, 2001), pp. 515–520.
25. For $C = 1$ pF and $I_0 = 0.77$ μA, the bare plasma frequency of the large junction is $\omega_p/2\pi \cong 8$ GHz, well below ν_{01}.
26. A. Cottet *et al.*, in *Macroscopic Quantum Coherence and Quantum Computing*, D. V. Averin, B. Ruggiero, P. Silvestrini, Eds. (Kluwer Academic, Plenum, New York, 2001), pp. 111–125.
27. I. I. Rabi, *Phys. Rev.* **51**, 652 (1937).
28. N. F. Ramsey, *Phys. Rev.* **78**, 695 (1950).
29. In practice, the rotation axis does not need to be x, but the rotation angle of the two pulses is always adjusted so as to bring a spin initially along z into the plane perpendicular to z.
30. At fixed Δt, the switching probability displays a decaying oscillation as a function of detuning.
31. H. Wolf *et al.*, *IEEE Trans. Instrum. Meas.* **46**, 303 (1997).
32. F. C. Wellstood, C. Urbina, J. Clarke, *Appl. Phys. Lett.* **50**, 772 (1987).

33. The indispensable technical work of P. Orfila is gratefully acknowledged. This work has greatly benefited from direct inputs from J. M. Martinis and Y. Nakamura. The authors acknowledge discussions with P. Delsing, G. Falci, D. Haviland, H. Mooij, R. Schoelkopf, G. Schön, and G. Wendin. Partly supported by the European Union through contract IST-10673 SQUBIT and the Conseil Général de l'Essone through the EQUM project.

26 December 2001; accepted 20 March 2002

Coherent Temporal Oscillations of Macroscopic Quantum States in a Josephson Junction

Yang Yu,[1] Siyuan Han,[1]* Xi Chu,[2]† Shih-I Chu,[2] Zhen Wang[3]

We report the generation and observation of coherent temporal oscillations between the macroscopic quantum states of a Josephson tunnel junction by applying microwaves with frequencies close to the level separation. Coherent temporal oscillations of excited state populations were observed by monitoring the junction's tunneling probability as a function of time. From the data, the lower limit of phase decoherence time was estimated to be about 5 microseconds.

The question of whether macroscopic variables obey quantum mechanics has stimulated extensive theoretical interests (*1*, *2*). The experimental search for macroscopic quantum phenomena (MQP) did not start until the early 1980s, when theory showed that the experimental conditions for observing MQP in Josephson junction–based devices were achievable (*3–5*). Many MQP, such as macroscopic quantum tunneling (MQT) (*6–10*), energy level quantization (*11*, *12*), quantum incoherent relaxation (*13*), resonant tunneling and photon-assisted tunneling (*14*), and photo-induced transition and population inversion between macroscopic quantum states (*15*, *16*), have since been observed. Recent spectroscopy evidence of superposition of fluxoid states and persistent-current states in superconducting quantum interference devices has also been reported (*17*, *18*). However, time domain coherent oscillations between macroscopic quantum states (MQS), which is more direct evidence for the superposition of MQS, has thus far evaded experimental detection.

One of the methods proposed to create coherent temporal oscillations between two MQS is via Rabi oscillation, an effect that is well established and understood in atomic and molecular systems (*19*). The principle of Rabi oscillations is that by applying a monochromatic electromagnetic (EM) field to a quantum two-level system, which interacts with the EM fields, the system will be in a superposition of the two energy eigenstates that results in oscillations between the lower and upper levels with Rabi frequency Ω. The amplitude of the population oscillations is at a maximum when the frequency of the EM wave ω is in resonance with the level spacing ΔE, i.e., $\omega = \Delta E/\hbar$. Rabi oscillation is a coherent quantum phenomenon that provides the foundation to a wide variety of basic research and applications, ranging from coherent excitation of atoms and molecules by laser to quantum computation (*20–22*). Re-

[1]Department of Physics and Astronomy, [2]Department of Chemistry, University of Kansas, Lawrence, KS 66045, USA. [3]Kansai Advanced Research Center, Communication Research Laboratory, Ministry of Posts and Telecommunications, 588-2 Iwaoka, Iwaoka-cho, Nishi-ku, Kobe, 651-24 Japan.

*To whom correspondence and requests should be addressed. E-mail: han@ku.edu

†Present address: Institute for Theoretical Atomic and Molecular Physics, Harvard-Smithsonian Center for Astrophysics, 60 Garden Street, Cambridge, MA 02138, USA.

cently, Rabi oscillations have been observed in mesoscopic systems such as quantum dots and wells and single Cooper pair tunneling devices (*23–27*). We report experimental evidence for Rabi oscillations in a macroscopic quantum system, a Josephson junction (JJ).

In order to observe Rabi oscillations in a macroscopic quantum system, the decoherence time τ_d must be significantly greater than the period of Rabi oscillations. This requirement is readily satisfied in atomic and molecular systems but is very difficult to meet in macroscopic systems, such as Josephson junctions, because of the coupling that occurs between the macroscopic variables and the environmental degrees of freedom. Using a Josephson tunnel junction that is carefully shielded from noises and weakly coupled to its environment, we were able to generate and detect Rabi oscillations between the MQS of the junction. The result is a clear demonstration of the superposition of macroscopic quantum states, a necessary requirement for the realization of pulse-driven superconducting quantum gates (*20*, *22*).

The dynamics of a JJ is equivalent to that of a fictitious particle of mass C moving in a washboard potential $U(\Phi) = -I_b\Phi - E_J\cos(2\pi\Phi/\Phi_0)$, where C is the junction capacitance, $\Phi_0 \equiv h/2e$ is the flux quantum, $E_J \equiv I_c\Phi_0/2\pi$ is the magnitude of maximum Josephson coupling energy, I_c is the critical current of the junction, I_b is the bias current, and $\Phi \equiv (\delta/2\pi)\Phi_0$ (where δ is the gauge-invariant phase difference of the superconducting order parameter across the junction) (*28*). An underdamped JJ with $I_b < I_c$ has two distinctive voltage states: The zero-voltage state corresponds to the particle being trapped in a metastable potential well, and the finite voltage state corresponds to the particle running down the washboard potential. It is also well established that underdamped JJ's have quantized energy levels and that microwaves can excite transitions between these levels (*9*, *11*, *12*). For a JJ pumped by microwaves, Rabi oscillations are expected to occur for $\tau_d \gg 2\pi/\Omega$. In the opposite limit of $\tau_d \ll 2\pi/\Omega$, the dynamics is incoherent and no coherent oscillations will occur.

Being able to generate Rabi oscillations in a JJ is not sufficient for their observation. In addition, one must also be able to detect them. We used the tunneling rate from the potential well to probe population ρ_{11} of the upper level $|1\rangle$. Because the tunneling rate from level $|1\rangle$ is more than 10^3 times that from level $|0\rangle$, the total tunneling rate is strongly influenced by ρ_{11}. In addition to tunneling, there are also the processes of interlevel decay and dephasing that affect the dynamics of the junction. The situation is depicted in Fig. 1, where Γ_i denotes the tunneling rate from level $|i = 0, 1\rangle$ and γ_{10} denotes the rate of energy relaxation from $|1\rangle$ to $|0\rangle$. Because the tunneling rates depend exponentially on the barrier height, the bias currents can be chosen so that the tunneling from $|0\rangle$ is essentially "frozen out" and escapes are mostly from the upper levels. Therefore, the time-dependent tunneling probability probes the temporal variation of the upper level population directly.

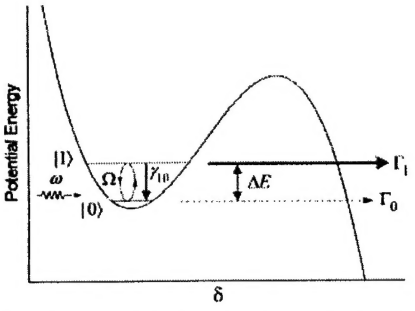

Fig. 1. An illustration of various coherent and incoherent processes in a metastable quantum two-level system radiated by a microwave. The model is applicable to a Josephson junction radiated by a monochromatic microwave.

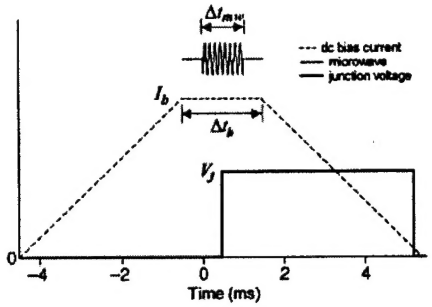

Fig. 2. An illustration of the timing of the dc current bias, microwave, and junction voltage. The junction's average lifetime in the zero-voltage state is much shorter than the microwave pulse duration, Δt_{mw}.

In the rotating wave approximation, the quantum dynamics of a Josephson junction with microwave excitations, including the effects of various decaying rates (Fig. 1), is described by the Liouville equation of the time evolution of the density matrix operator

$$\frac{du}{dt} = \Delta v(t) - \Gamma u(t), \quad (1)$$

$$\frac{dv}{dt} = -\Delta u(t) - \Gamma v(t) + \Omega_0 w(t), \quad (2)$$

$$\frac{dw}{dt} = -\frac{1}{2}(\Gamma_1 + 2\gamma_{10} + \Gamma_0)w(t) - \Omega_0 v(t) - \frac{1}{2}(\Gamma_1 + 2\gamma_{10} - \Gamma_0)S(t), \quad (3)$$

$$\frac{dS}{dt} = -\frac{1}{2}(\Gamma_1 + \Gamma_0)S(t) - \frac{1}{2}(\Gamma_1 - \Gamma_0)w(t) \quad (4)$$

where $\Delta = (E_1 - E_0)/\hbar - \omega$ is the detuning (with ω the microwave frequency), $\Omega_0 = |\delta_{01} i_{rf} E_J/\hbar|$ is the on-resonance ($\Delta = 0$) Rabi frequency, i_{rf} is the amplitude of microwave current normalized to I_c, $\delta_{01} = \langle 0|\delta|1\rangle$ is the coupling matrix element, $u = \rho_{01} + \rho_{10}$, $v = \frac{1}{i}(\rho_{01} - \rho_{10})$, $w = \rho_{11} - \rho_{00}$, and $S = \rho_{11} + \rho_{00}$. In addition, we have defined $\Omega \equiv \sqrt{\Omega_0^2 - (\Gamma - i\Delta)^2}$ as the Rabi frequency and Γ as the total off-diagonal decay rate given by $\Gamma = \frac{1}{2}(\Gamma_1 + \Gamma_0 + \gamma_{10}) + \gamma_\varphi$ (with γ_φ as the dephasing rate). The set of Liouville equations can be solved analytically by means of the Laplace transformation technique, from which the time-dependent populations of both levels can be obtained. The exact analytical solutions are too cumbersome to present here. However, in the limit of $\Gamma_1 > \gamma_{10} > \gamma_\varphi > \Gamma_0$, a situation likely to be applicable here, we obtain the approximate analytical solution as follows

$$\rho_{11}(t) = e^{-\Gamma t}\frac{\Omega_0^2}{|\Omega^2|}\left|\sin\left(\frac{\Omega t}{2}\right)\right|^2 \quad (5)$$

which describes damped oscillations, in contrast to the simple exponential decay behavior of incoherent processes.

We used a 10 μm by 10 μm NbN/AlN/NbN junction. The junction parameters, $I_c \approx 147.9$ μA and $C = 5.8 \pm 0.6$ pF, were obtained from independent measurements in the thermal regime. I_c and C, together with I_b, uniquely determine the energy level separations. All electrical leads connected to the junction are carefully filtered. The measured switching current distributions of junctions on the same chip but with much smaller critical current were consistent with the prediction of MQT theory to $T = 8$ mK, indicating that the effect of extrinsic noises was negligible. A more detailed description of our experimental setup can be found elsewhere (*29*). Because the junction was inside a high Q (high quality factor) cavity, it was difficult to sweep the microwave frequency while keeping constant the power coupled to the junction. Therefore, varying detuning parameter Δ was accomplished by changing the junction's dc bias current $i_b \equiv I_b/I_c$ (thus the level separation) while keeping ω constant. Another important property of the system is that the tunneling rate is sensitive to the applied microwave power. If the power is too high, it will cause significant strong field effects (e.g., multiphoton transitions). Conversely, weaker microwave power results in smaller amplitude of Rabi oscillations due to the finite detuning.

The measurement of the time evolution of

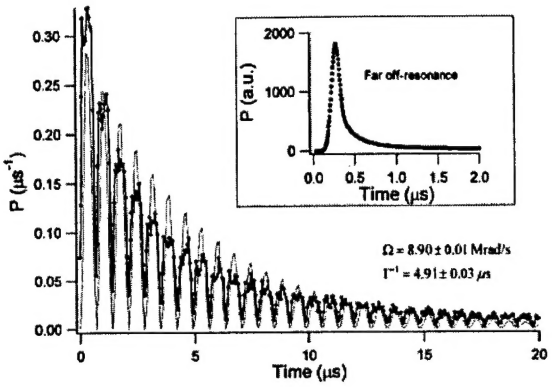

Fig. 3. Tunneling probability density $P(t)$ measured at 8 mK at $i_b \simeq 0.993$ with the microwave frequency set to $f = 16.500$ GHz. The frequency detuning Δ is estimated to be less than 5 Mrad/s, and the on-resonance Rabi frequency is $\sim\Delta$. The circles (connected by the black line to guide eyes) are data and the solid line is the best fit to Eq. 5. (Inset) Data taken at a slightly higher dc bias current where the detuning value is much larger.

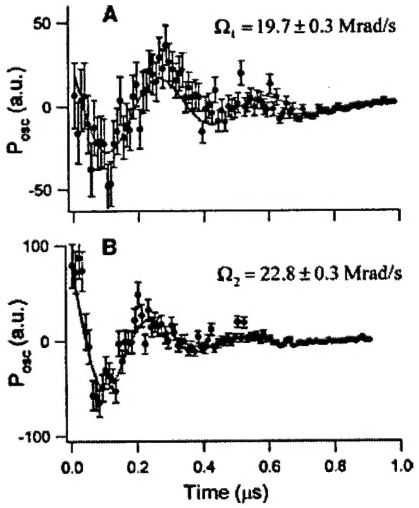

Fig. 4. Microwave power dependence of Rabi frequency with **(A)** 7.8 pW and **(B)** 10 pW injected to the sample cell. The circles are data and the red solid lines are the best fit to the oscillatory part of Eq. 6. The higher bias current $i_b \simeq 0.994$ results in a faster exponential decay (see Eq. 5).

tunneling probability density $P(t)$ is as follows: for each measurement cycle, the junction's bias current was ramped up to and kept at I_b for a period of Δt_b (Fig. 2). At this bias level, typically around $i_b \gtrsim 0.99$, the average time remaining in the zero-voltage state without microwave is much greater than Δt_b so that almost no escape would occur at $t < \Delta t_b$. A microwave pulse of frequency $f = \omega/2\pi$ and duration Δt_{mw} was then applied (Fig. 2) to the junction via a cryogenic semirigid coaxial cable, which generates oscillations in upper-level population and thus a periodic enhancement of the tunneling rate. The time at which the junction switched from the zero to finite voltage state, the escape time, was recorded using a timer with subnanosecond resolution. The process was repeated 10^4 to 10^5 times. The tunneling probability density $P(t)$, the number of tunneling events per unit time, was then obtained from the histogram of escape times. $P(t)$ is approximately proportional to ρ_{11} for $\Gamma_0 \ll \Gamma_1$. With the limit of $\Delta = 0$ and fast decay, Eq. 5 becomes

$$\rho_{11}(t) = e^{-\Gamma t}\frac{\Omega_0^2}{2|\Omega^2|}(1-\cos\Omega t) \qquad (6)$$

In Fig. 3, the measured tunneling probability density is shown as a function of time. The frequency and duration of the microwave pulses are $\omega/2\pi = 16.5$ GHz and $\Delta t_{mw} = 0.1$ ms. Because all tunneling events occurred at $t < \Delta t_{mw}$, the effect of microwave pulse is the same as that of a continuous wave turned on at $t = 0$. The measured $P(t)$ clearly shows the damped temporal oscillations described by Eq. 5. The peaks and dips in $P(t)$ correspond to the population of excited state reaching maxima and minima, respectively. The period of oscillations and the decay time, obtained from fitting the data to Eq. 5, are $\Omega = 8.90 \pm 0.01$ megarad/s and $\Gamma^{-1} = 4.91 \pm 0.03$ μs. However, observation of damped $P(t)$ oscillations is necessary but not sufficient evidence of Rabi oscillation because the oscillations can also be due to other mechanisms. For instance, the observed oscillations could be caused by frequency beats between the applied microwave and a cavity mode, which would lead to $P(t)$ oscillations with frequency $\Delta\omega \equiv \omega - \omega_{cav}$, where ω_{cav} is the frequency of the cavity mode. In this case $P(t)$ would not be sensitive to variations in detuning Δ when $\Delta\omega$ was fixed. In contrast, for weak microwave fields, the amplitude of $P(t)$ oscillations due to Rabi mechanism depends strongly on the detuning Δ. Therefore, the Δ dependence of $P(t)$ can be used to verify whether the observed oscillations were due to the cavity-microwave interaction. To do this, $P(t)$ was measured at a slightly higher bias current i_b while keeping all other parameters the same. There are two major effects of increasing i_b. One of them is to reduce the level spacing, thus increasing the detuning Δ; the other is to increase the tunneling rate so that the total off-diagonal decay rate Γ would be much greater. The inset of Fig. 3 shows what happened when the dc bias current was increased by a very small amount of $\delta i_b \lesssim 2 \times 10^{-3}$. It can be seen that oscillations in $P(t)$ were washed out and the overall tunneling rate was much higher. The observed Δ dependence is, therefore, inconsistent with the cavity-microwave interaction mechanism.

In the limit of small detuning $\Delta \ll \Omega$, Eq. 5 predicts that the frequency of ρ_{11} oscillations, and hence the tunneling probability, is proportional to the amplitude of the microwave. Therefore, when the amplitude of the microwave is changed from A_1 to A_2, the frequency of Rabi oscillations should vary in accordance with $\Omega_1/\Omega_2 \simeq A_1/A_2$. The relation provides a very useful test for Rabi oscillations in the Josephson junction. Although the absolute values of microwave amplitude coupled to the junction could not be determined by our experiment, the ratio A_1/A_2 was precisely determined. Figure 4 shows the oscillatory part of the excited state population P_{osc} as a function of time with two different microwave power levels. The data were taken at $i_b \simeq 0.994$, $\omega/2\pi = 16.000$ GHz, and with $A_1/A_2 = 0.88$. As microwave power was increased the angular frequency of the oscillations, obtained from the best fits, increased from $\Omega_1 = 19.7 \pm 0.3$ megarad/s to $\Omega_2 = 22.8 \pm 0.3$ megarad/s. The ratio $\Omega_1/\Omega_2 = 0.864 \pm 0.025$ is in good agreement with the theory. Therefore, we conclude that the observed oscillations were due to microwave excited coherent Rabi oscillations between the macroscopic quantum states of the JJ.

Our result demonstrates the coherent superposition and temporal oscillations of macroscopic quantum states in a JJ, which has important implications for quantum state engineering of Josephson devices and quantum computation with the use of superconducting qubits. For instance, one of the most important properties of these qubits is the phase decoherence time $\tau_\varphi \equiv \gamma_\varphi^{-1}$, which sets the time scale over which phase coherence can be maintained. In our experiment, the decay time constant $\tau = \Gamma^{-1}$ sets a lower limit for τ_φ because Γ is always greater than γ_φ. From the data (Fig. 3), we estimated that the phase decoherence time is greater than 4.9 μs, which is consistent with the previous result of post-pulse escape rate measurements (*29*). Lastly, being able to generate Rabi oscillations in Josephson junctions greatly enhances the prospects of realizing quantum computation with microwave pulse-driven superconducting qubits (*20–22*).

References and Notes

1. E. Schrödinger, *Naturwissenschaften* **23**, 844 (1935).
2. A. J. Leggett, A. Garg, *Phys. Rev. Lett.* **54**, 857 (1985).
3. A. O. Caldeira, A. J. Leggett, *Phys. Rev. Lett.* **46**, 211 (1981).
4. A. J. Leggett, *Quantum Tunneling in Condensed Media*, vol. 34 of *Modern Problems in Condensed Matter Sciences*, Y. Kagan, A. J. Leggett, Eds. (North-Holland, Amsterdam, 1992) chap. 1, pp. 1–36.
5. A. J. Leggett *et al.*, *Rev. Mod. Phys.* **59**, 1 (1987).

6. R. F. Voss, R. A. Webb, *Phys. Rev. Lett.* **47**, 265 (1981).
7. S. Washburn, R. A. Webb, R. F. Voss, S. M. Faris, *Phys. Rev. Lett.* **54**, 2712 (1985).
8. D. B. Schwartz, B. Sen, C. N. Archie, J. E. Lukens, *Phys. Rev. Lett.* **55**, 1547 (1985).
9. J. Clarke, A. N. Cleland, M. H. Devoret, D. Esteve, J. M. Martinis, *Science* **239**, 992 (1988).
10. M. H. Devoret, J. M. Martinis, J. Clarke, *Phys. Rev. Lett.* **55**, 1908 (1985).
11. J. M. Martinis, M. H. Devoret, J. Clarke, *Phys. Rev. Lett.* **55**, 1543 (1985).
12. P. Silvestrini, V. G. Palmieri, B. Ruggiero, M. Russo, *Phys. Rev. Lett.* **79**, 3046 (1997).
13. S. Han, J. Lapointe, J. E. Lukens, *Phys. Rev. Lett.* **66**, 810 (1991).
14. R. Rouse, S. Han, J. E. Lukens, *Phys. Rev. Lett.* **75**, 1614 (1995).
15. S. Han, R. Rouse, J. E. Lukens, *Phys. Rev. Lett.* **76**, 3404 (1996).
16. ———, *Phys. Rev. Lett.* **84**, 1300 (2000).
17. J. R. Friedman, V. Patel, W. Chen, S. K. Tolpygo, J. E. Lukens, *Nature* **406**, 43 (2000).
18. C. H. van der Wal *et al.*, *Science* **290**, 773 (2000).
19. I. I. Rabi, *Phys. Rev.* **51**, 652 (1937).
20. S. Lloyd, *Science* **261**, 1569 (1993).
21. M. F. Bocko, A. M. Herr, M. J. Feldman, *IEEE Trans. Appl. Supercond.* **7**, 3638 (1997).
22. Y. Makhlin, G. Schön, A. Shnirman, *Rev. Mod. Phys.* **73**, 357 (2001).
23. T. H. Stievater *et al.*, *Phys. Rev. Lett.* **87**, 133603 (2001).
24. R. H. Blick, D. W. van der Weide, R. J. Haug, K. Eberl, *Phys. Rev. Lett.* **81**, 689 (1998).
25. C. A. Stafford, N. S. Wingreen, *Phys. Rev. Lett.* **76**, 1916 (1996).
26. A. Schülzgen *et al.*, *Phys. Rev. Lett.* **82**, 2346 (1999).
27. Y. Nakamura, Y. A. Pashkin, J. S. Tsai, *Phys. Rev. Lett.* **87**, 246601 (2001).
28. A. Barone and G. Paterno, *Physics and Applications of the Josephson Effect* (John Wiley and Sons, New York, 1982) pp. 1–14.
29. S. Han, Y. Yu, X. Chu, S. Chu, Z. Wang, *Science* **293**, 1457 (2001).
30. We thank Y. Zhang and S. Li for technical assistance in preparing the experiment. S.H. thanks J. E. Lukens for useful discussions. Supported in part by NSF (DMR-9876874 and EIA-0082499) and by Air Force Office of Scientific Research (AFOSR) (grant F49620-01-1-0439), funded under the Department of Defense University Research Initiative on Nanotechnology (DURINT) program and by the Advanced Research and Development Activity (ARDA).

2 January 2002; accepted 15 March 2002

Ordering of Quantum Dots Using Genetically Engineered Viruses

Seung-Wuk Lee, Chuanbin Mao, Christine E. Flynn, Angela M. Belcher*†

A liquid crystal system was used for the fabrication of a highly ordered composite material from genetically engineered M13 bacteriophage and zinc sulfide (ZnS) nanocrystals. The bacteriophage, which formed the basis of the self-ordering system, were selected to have a specific recognition moiety for ZnS crystal surfaces. The bacteriophage were coupled with ZnS solution precursors and spontaneously evolved a self-supporting hybrid film material that was ordered at the nanoscale and at the micrometer scale into ~72-micrometer domains, which were continuous over a centimeter length scale. In addition, suspensions were prepared in which the lyotropic liquid crystalline phase behavior of the hybrid material was controlled by solvent concentration and by the use of a magnetic field.

Building ordered and defect-free two- and three-dimensional structures on the nanometer scale is essential for the construction of next-generation optical, electronic, and magnetic materials and devices (*1–4*). Traditional assembly approaches have been based on hydrogen bonding, coulombic interactions, and van der Waals forces (*1, 4*). Although a bacterial synthetic method was reported to make monodisperse modified polypeptides (*5*), it has been difficult to tune the layer spacing and structure of conventional synthetic polymers because of their polydisperse chain lengths (*6*). Efforts have been directed toward the use of soft materials to organize inorganic materials at the nanoscale. Protein cages have been used as templates to synthesize nanoscale materials in capsids (*7*). DNA recognition linkers have been successfully used to construct specific gold nanocrystal structures (*8, 9*). ZnS and CdS were nucleated in a lyotropic liquid crystalline medium to make nanowires and nanocrystal superlattice structures by a surfactant assembly pathway (*10*). However, these methods have limitations with respect to length scale and type of inorganic material.

Monodisperse biomaterials that have an anisotropic shape are promising as components of well-ordered structures. Liquid crystalline structures of wild-type viruses (Fd, M13, and TMV) were tunable by controlling the solution concentrations, the solution ionic strength, and the external magnetic fields applied to the solutions (*11–14*). We recently showed that engineered viruses can recognize specific semiconductor surfaces through the method of selection by combinatorial phage display (*15*). These specific recognition properties of the virus can be used to organize inorganic nanocrystals, forming ordered arrays over the length scale defined by liquid crystal formation. We have evolved phage and ZnS precursor solutions to self-assemble highly oriented, self-supporting films. In this system, we can easily modulate both the length of bacteriophage and the type of inorganic materials through genetic modification and selection. Here we report our first effort to direct multi–length scale ordering of quantum dot (QD) hybrid self-supporting biocomposite structures using genetically engineered M13 bacteriophage, viruses with monodisperse size and shape. The resulting QD hybrid film material was ordered at the nanoscale and at the micrometer scale into 72-μm domains. These domains repeated continuously over a centimeter length scale. Moreover, viral suspensions containing ZnS QDs were prepared in which the liquid crystalline phase behaviors of the hybrid material were controlled by solvent concentration and by the use of an applied magnetic field.

The most dominant selected peptide binding motif with specific recognition of ZnS crystal surfaces was isolated through screening of phage display libraries (Fig. 1) (*16, 17*). The screening method selected for binding affinity of a population of random peptides displayed as part of the pIII minor coat protein of M13. Selected peptides were expressed at one end of the M13 virus. The virus had a filamentous shape (~880 nm in length and 6.6 nm in diameter), with the peptide insert measuring 10 nm in length (*11*). The dominant binding motif that emerged after five rounds of selection was termed A7, with an amino acid insert sequence (Cys-Asn-Asn-Pro-Met-His-Gln-Asn-Cys) in which the two cysteine groups formed a disulfide bond, restricting the peptide structure to a constrained loop (*16*). The peptide expressed on the virus was tested and confirmed to have binding specificity to ZnS crystal surfaces (*16, 18*). The bacteriophage containing this A7 peptide—termed A7 phage—was cloned and amplified to liquid crystalline concentrations, with DNA verification after each amplification step.

The A7 phage was precipitated and then resuspended in ZnS precursor solutions to form an A7 phage–ZnS nanocrystal (A7-ZnS) liquid crystalline suspension (*19*). The liquid crystalline behavior of the suspensions was dominated by the long-rod phage shape, despite the at-

Department of Chemistry and Biochemistry, Center for Nano- and Molecular Science and Technology, Texas Materials Institute, Institute for Cellular and Molecular Biology, University of Texas at Austin, Austin, TX 78712, USA.

*Present address: Department of Materials Science and Engineering and Biological Engineering, Massachusetts Institute of Technology, Cambridge, MA 02139, USA.

†To whom correspondence should be addressed. E-mail: belcher@mit.edu